THEMED ISSUE: Ophiolites, Diamonds, and UHP Minerals: New Discoveries and Concepts on Upper Mantle Petrogenesis

THE GEOLOGICAL SOCIETY OF AMERICA®

Seafloor spreading structure, geochronology, and tectonic evolution of the Küre ophiolite, Turkey: A Jurassic continental backarc basin oceanic lithosphere in southern Eurasia

Gözde Alparslan and Yildirim Dilek*
DEPARTMENT OF GEOLOGY AND ENVIRONMENTAL EARTH SCIENCE, MIAMI UNIVERSITY, 208 SHIDELER HALL, 250 S. PATTERSON AVENUE, OXFORD, OHIO 45056, USA

ABSTRACT

The Küre ophiolite in the Sakarya terrane in northern Anatolia is a Penrose-type ophiolite, complete with a sheeted dike complex, and includes well-developed volcanogenic massive sulfide deposits. It is tectonically imbricated along south-directed thrust faults between the Paleozoic, continental basement rocks of the Devrekani Massif (Eurasia) to the north and the Late Triassic–Early Cretaceous subduction-accretion complexes (Tethys) to the south. The ~5-km-thick crustal lithologies in the ophiolite are crosscut by west-northwest–east-southeast–oriented, extensional ductile-brittle shear zones and normal faults that display hydrothermal mineralization and seafloor alteration effects. The west-northwest–east-southeast–striking sheeted dikes and these extensional fault systems indicate a north-northeast–south-southwest seafloor spreading direction during the magmatic evolution of the ophiolite. The U-Pb zircon dating of a gabbroic rock has revealed a concordant age of 168.8 ± 2 Ma that represents the timing of the igneous construction of the ophiolite. Sandstone units in the ~3-km-thick turbiditic sedimentary cover of the ophiolite contain Paleoarchean, Neoarchean, and Proterozoic detrital zircons, derived from the Ukrainian shield and the East European Platform, indicating a proximal position of the Küre basin to Eurasia during its development. The Küre ophiolite represents a Middle Jurassic continental backarc basin ophiolite with a Eurasian affinity.

LITHOSPHERE; v. 10; no. 1; p. 14–34; GSA Data Repository Item 2018054 | Published online 5 January 2018 https://doi.org/10.1130/L641.1

INTRODUCTION

Ophiolites represent on-land fragments of the ancient oceanic lithosphere and are archives displaying structural, petrological, and geochemical evidence for the mode and nature of Earth processes occurring during the construction of oceanic crust (Moores, 1982; Dilek and Furnes, 2011, 2014). They are composed of spatially and temporally associated ultramafic, mafic, and felsic rock suites that collectively make up the oceanic crust and upper mantle assemblages of former ocean basins (Anonymous, 1972; Dilek and Delaloye, 1992). Tectonic and geochemical fingerprinting of ophiolites has shown that these ultramafic-mafic-sedimentary rock assemblages may have formed in diverse tectonic settings during the evolution of ancient ocean basins from their rift-drift and seafloor spreading stages to subduction initiation and final closure phases (Dilek and Furnes, 2011).

Backarc basin ophiolites make up one of the most widespread ophiolite types in the rock record (Furnes et al., 2014). Their magmatic construction takes place in trench-proximal or trench-distal spreading centers behind active volcanic arc systems within a suprasubduction zone environment (Dilek and Furnes, 2014). Backarc basin extension and spreading-related oceanic crust formation may occur in both oceanic and continental settings, as observed in the modern Izu-Bonin-Mariana intraoceanic arc and the Sea of Japan continental backarc basin examples. In these settings, fast subduction and rapid slab rollback rates appear to have played a major role in the mode of backarc basin opening (Jolivet et al., 1994; Schellart and Lister, 2005; Sdrolias and Müller, 2006; Holt et al., 2015). The distance of backarc spreading center from an active trench and the oceanic versus continental basement setting of its origin strongly affect the geochemical signatures of crustal rocks and the types of sedimentary cover sequences (Hawkins, 2003). These characteristics of modern backarc basin oceanic rocks are generally well preserved in ophiolites and provide important clues to decipher the nature of paleo–subduction zone processes, subduction polarities, and timing and nature of basin closure and inversion in studying orogenic belts (Flower, 2003). However, most backarc ophiolites are highly deformed and fragmented during basin closure, ophiolite emplacement, and subsequent collisional processes, such that their seafloor spreading structures and three-dimensional crustal architecture are largely obliterated.

In this paper we report on the internal structure, geochronology, and regional geology of the Küre ophiolite in north-central Anatolia (Turkey; Fig. 1), a well-preserved, complete Penrose-type ophiolite (see Anonymous, 1972, and Dilek, 2003b, for the definition of a Penrose-type ophiolite). Its magmatic and tectonic evolution within the Tethyan tectonic framework is not well understood, in part due to the lack of any radiometric or isotopic age data from its crustal units. We first document the seafloor spreading–related crustal architecture of the Küre ophiolite and the nature, geometry, and kinematics of contractional deformation structures that

Yildirim Dilek http://orcid.org/0000-0003-2387-9575
*Corresponding author: dileky@miamioh.edu

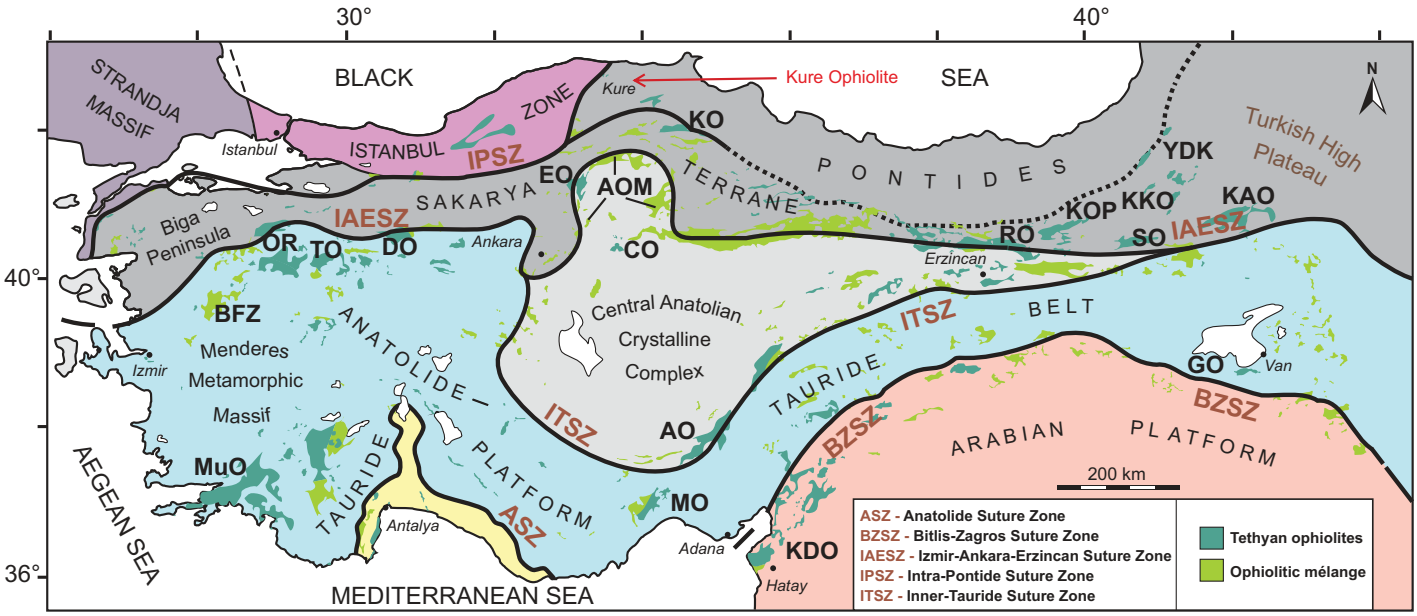

Figure 1. Simplified tectonic map of Anatolia, showing the major tectonic belts, collisional suture zones, and Tethyan ophiolites and ophiolitic mélange zones. Abbreviations for different ophiolites and ophiolitic mélanges: AO—Aladağ ophiolite; AOM—Ankara ophiolitic mélange; BFZ—Bornova flysch zone; CO—Çiçekdağ ophiolite; DO—Dağküplü ophiolite; EO—Eldivan ophiolite; KAO—Kağızman ophiolite; KDO—Kızıldağ ophiolite; KO—Kargı ophiolite; KOP—Kop ophiolite; KKO—Kırdağ-Karadağ ophiolite; MO—Mersin ophiolite; MuO—Muğla ophiolite; OR—Orhaneli ophiolite; RO—Refahiye ophiolite; SO—Sahvelet ophiolite; TO—Tavsanlı ophiolite (data from Okay and Tüysüz, 1999; Dilek and Whitney, 2000; Dilek et al., 2010; Sarıfakıoğlu et al., 2017).

formed during the basin closure. We present new U-Pb zircon dates from a gabbroic rock and from a sandstone unit in the sedimentary cover, and preliminary geochemical data and interpretations from its extrusive rock units. These new observations and data collectively allow us to constrain the magmatic age of the ophiolite, the detrital provenance of its ocean basin, and the tectonic setting of its formation within the Eurasian realm. Our results suggest that the Küre ophiolite represents a continental backarc basin oceanic lithosphere in the global ophiolite record.

REGIONAL GEOLOGY

Tethyan ophiolites in Anatolia occur along a series of nearly east-west–trending suture zones (Fig. 1), which developed as various Tethyan seaways, separated by Gondwana-derived microcontinents, during the Mesozoic–early Cenozoic (Dilek and Moores, 1990; Dilek et al., 1999; Robertson, 2002; Dilek, 2003a; Shallo and Dilek, 2003; Göncüoglu et al., 2012; Marroni et al., 2014). In general, there is an age progression of these suture zones and the associated oceanic remnants (ophiolites and mélanges) from north to south; the oldest ophiolites are exposed along the Intra-Pontide suture zone (IPSZ) in the north and the youngest ones are along the Bitlis-Zagros suture zone along the northern periphery of the Arabian Platform to the south (Fig. 1; Dilek, 2006). The IPSZ contains the remnants of a Late Triassic–Cretaceous ocean basin (Elmas and Yiğitbaş, 2001; Moix et al., 2008; Göncüoglu et al., 2012; Akbayram et al., 2013; Marroni et al., 2014), and separates the Gondwana-derived Sakarya terrane in the south from the Istanbul zone of Eurasia in the north (Figs. 1 and 2). The closure of the Intra-Pontide Ocean resulted in the collision of the Istanbul zone and the Sakarya terrane in the Early Jurassic and then in the southward accretional growth of Eurasia before the end of the Middle Jurassic.

The Küre ophiolite occurs within the Sakarya terrane in the Pontide tectonic belt in northern Anatolia (Fig. 1). It is nearly 100 km north of the IPSZ and within an intracontinental setting along the southern edge of Eurasia. It is therefore a tectonic outlier well outside of the nearest collisional suture zone. We briefly summarize here the tectonic components of the Pontide belt and the Sakarya terrane to provide a regional geological context for the Küre ophiolite.

Pontide Tectonic Belt

The Pontide belt consists of three nearly east-west–trending terranes, which include, from north to south, the Strandja Massif, the Istanbul zone, and the Sakarya terrane (Fig. 1). The Strandja Massif consists of Precambrian–early Paleozoic quartzofeldspathic gneisses that are intruded by late Carboniferous–early Permian (257 ± 6 Ma) granitoids (Sunal et al., 2006), and is part of a larger composite terrane, including the Rhodope and Serbo-Macedonian metamorphic Massifs in the Balkan Peninsula (Zagorchev, 2008). The Istanbul zone is a small continental fragment to the southwest of the Black Sea and includes a Precambrian crystalline basement and an Ordovician–Carboniferous passive margin sedimentary sequence, which is unconformably overlain by latest Permian–Triassic terrigenous rocks (Dean et al., 2000; Görür et al., 1997; Okay and Tüysüz, 1999). Cretaceous flysch deposits overlie these older basement units in the Istanbul zone. The Sakarya terrane is separated from the Anatolide-Tauride Platform to the south by the Izmir-Ankara-Erzincan suture zone (IAESZ) (Fig. 1). It is made of a Carboniferous metamorphic massif (gneiss, amphibolite, marble, metaperidotites), Paleozoic granitoids (Devonian and Permian–Carboniferous), and a Permian–Triassic subduction-accretion complex (Karakaya Complex) with Late Triassic blueschists and eclogites (Okay et al., 2002, and references therein), and Jurassic–Cretaceous arc, forearc, magmatic arc, and accretionary prism complexes (Tankut et al., 1998; Sarıfakıoğlu et al., 2017; Okay et al., 2014; this study).

Late Cretaceous volcanic and volcanogenic extrusive rocks, andesitic dikes and sills, and calc-alkaline plutons above and across these older

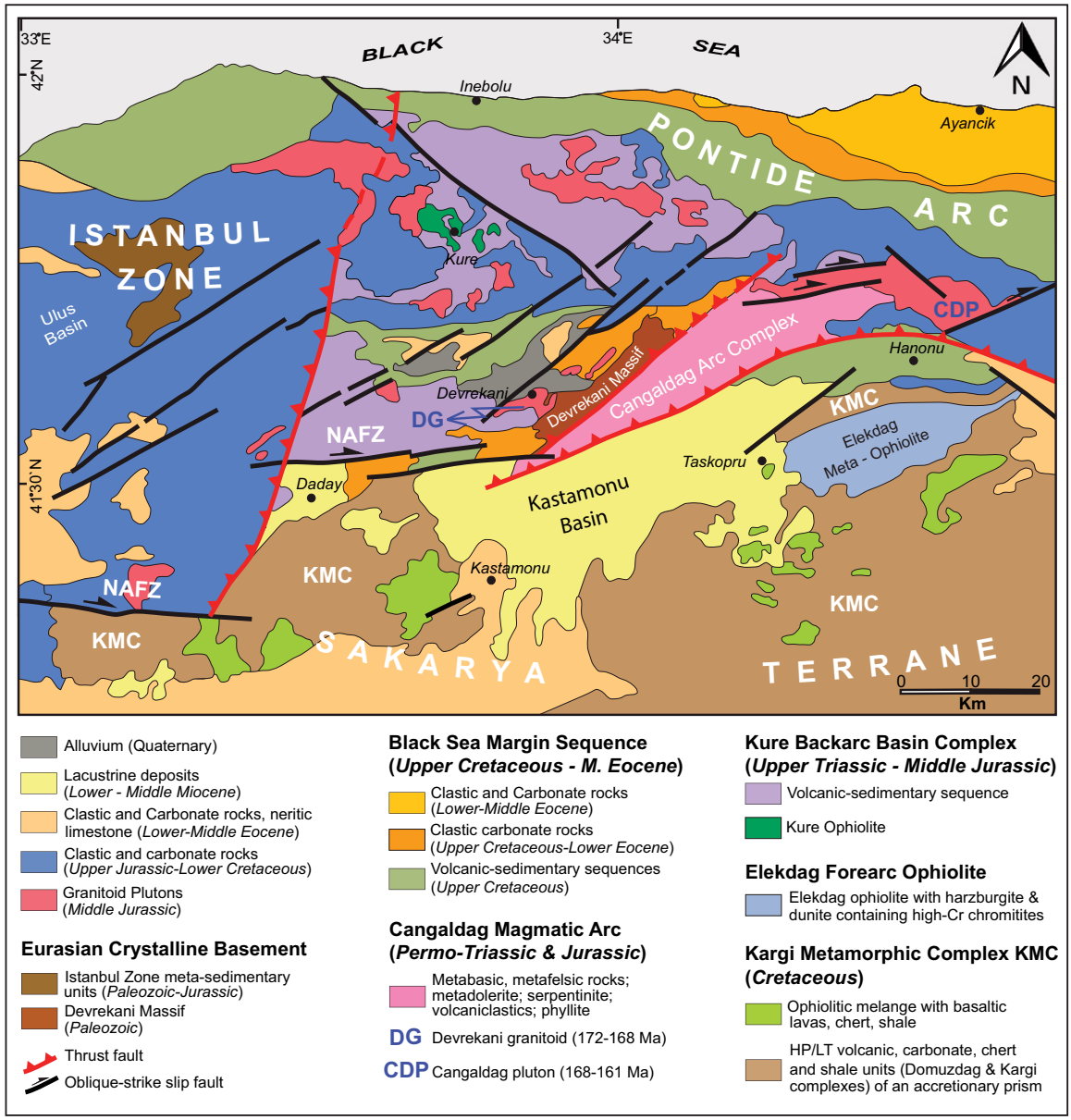

Figure 2. Tectonic map of the Central Pontide Belt in north-central Anatolia, showing its internal structure and tectonostratigraphy and the occurrence of the Küre ophiolite north of the Çangaldag magmatic arc. The northeast-southwest–striking en echélon oblique-slip faults are associated with strain partitioning along the northeast-southwest–extending North Anatolian fault zone (NAFZ). HP/LT—high pressure–low temperature.

terranes constitute an approximately east-west–trending magmatic arc (Pontide arc) that extends from Bulgaria in the west to the Republic of Georgia in the east. The Black Sea represents a backarc basin of the Pontide arc. The construction of the Pontide arc and the opening of the Black Sea backarc basin occurred above the Neotethyan oceanic slab, which was dipping northward beneath Eurasia during the Cretaceous (Robinson et al., 1995; Okay and Şahintürk, 1997). The region to the north and west of the Black Sea basin encompasses the East European Platform, which comprises Archean and Paleoproterozoic crystalline basement rocks, and Neoproterozoic crustal rocks (Okay and Nikishin, 2015). The Istanbul zone was located, prior to the opening of the Black Sea, south of the East European Platform, which was the southward extension of the Ukrainian shield in Eurasia (Nikishin et al., 2015).

Crustal Architecture of the Central Sakarya Terrane

The Küre ophiolite is tectonically imbricated along south-directed thrust faults between the Paleozoic Devrekani metamorphic massif to the south and the Paleozoic–Jurassic continental basement rocks of the Istanbul zone to the north (Fig. 2). The Devrekani Massif in the south-central part of the Sakarya terrane consists of Paleozoic gneiss, amphibolite, and marble, and tectonically overlies a Late Triassic–Jurassic volcanic-plutonic complex (Çangaldag Complex) to the south along a southeast-directed thrust fault (Fig. 2). The Devrekani Massif has been interpreted as a rifted fragment of the crystalline basement (Hercynian origin) of the Istanbul zone (Ustaömer and Robertson, 1994). The Çangaldag Complex includes Permian–Triassic metabasite and phyllite, overlain by Late

Triassic–Jurassic volcanic and volcaniclastic rocks, and intruded by Early–Middle Jurassic granitoid plutons (Ustaömer and Robertson, 1994; Okay et al., 2006). Two major granitoid plutons have been identified in the literature as part of the plutonic foundation of the Çangaldag Complex. One of these plutons, the Devrekani granitoid (Fig. 2), consists of low-K tholeiitic and medium-K calc-alkaline diorites and metaluminous granites (Nzegge, 2008). Its U-Pb zircon dating has revealed crystallization ages of 172–168 Ma (Nzegge, 2008). The other, the Çangaldag pluton, is in the northeast part of the Çangaldag Complex (Fig. 2). In situ U-Pb zircon dating of a granitic rock from this pluton has provided a crystallization age of 168.3 ± 2.1 (Çimen, 2016). The Çangaldag Complex is interpreted as a magmatic arc (Çangaldag arc complex) that developed along the southern edge of the Sakarya terrane and above a north-dipping subduction zone beneath Eurasia (Ustaömer and Robertson, 1994; Nzegge, 2008; Okay et al., 2014).

The Elekdag ophiolite south of the Çangaldag magmatic (Fig. 2) arc comprises serpentinized peridotites, layered to isotropic gabbros, sheeted dikes, and metalavas (Dönmez et al., 2014). There are no radiometric or isotopic ages currently available from the Elekdag ophiolite. The compositions of both high-Cr and high-Al chromitites associated with dunites in the Elekdag peridotites indicate their origin as a result of interactions of subduction-derived boninitic melts with depleted harzburgites in a forearc tectonic setting (Dönmez et al., 2014). Therefore, the Elekdag ophiolite is considered as a forearc oceanic lithosphere that developed in part synchronously with the Çangaldag magmatic arc (Ustaömer and Robertson, 1994; Dönmez et al., 2014). Some researchers have reported the occurrence of eclogites and high-pressure metabasites (blueschists) as thin thrust slices bounding the Elekdag ophiolite both to the north and to the south or within the ophiolite. Altherr et al. (2004) interpreted their existence as blocks within a highly sheared serpentinite matrix mélange, rather than as part of a coherent ophiolite pseudostratigraphy. Okay et al. (2006) showed these eclogite-blueschist occurrences as almost entirely restricted to the northern and southern shear zone boundaries of the Elekdag ophiolite with the Domuzdag complex, which contains garnet-blueschist, mica schist, eclogite, and metaophiolitic units. We interpret these eclogite-blueschist rocks as thrust-imbricated tectonic slices of the Domuzdag subduction-accretion complex, instead of being part of the Elekdag ophiolite. There are no reports in the literature, demonstrating that the Elekdag ophiolite units display a blueschist metamorphic overprint.

To the south of the Çangaldag-Elekdag magmatic arc-forearc tectonic system is the Kargi metamorphic complex, which consists largely of metapelitic rocks, imbricated by south-vergent, crustal-scale thrust faults, and thrust sheets of ophiolitic mélange units. These metasedimentary rocks are tectonically interleaved with blocks of garnet blueschist, mica schist, metagabbro, and eclogite that collectively make up the Domuzdag complex (Fig. 2; Okay et al., 2015). The Domuzdag complex is nearly 1 km thick, and its metamorphic rocks display steeply north-dipping penetrative foliation that is spatially associated with isoclinal folds (Okay et al., 2006). Rb-Sr phengite ages obtained from its eclogitic rocks have revealed high-pressure metamorphism ages between 124 ± 9 and 106 ± 3 Ma (Okay et al., 2015). The $^{40}Ar/^{39}Ar$ dating of an eclogitic rock revealed cooling ages ranging from 95.1 ± 0.6 to 116.5 ± 3.4 Ma, with a mean age of 104.5 ± 7.2 Ma (Okay et al., 2006). The ophiolitic mélange consists of blocks and lenses of highly deformed basaltic lavas, chert, dolerite, and gabbro in an intensely sheared serpentinite matrix. Metabasaltic lavas have a mid-oceanic ridge basalt (MORB) geochemical affinity (Ustaömer and Robertson, 1994; Altherr et al., 2004). High-pressure metamorphic rocks and the highly deformed and metamorphosed, serpentinized matrix, ophiolitic mélange in the Kargi metamorphic complex collectively represent a fossil subduction channel in the Tethyan subduction-accretion system at the active margin of southern Eurasia (Fig. 2; this study). The Domuzdag complex is locally unconformably overlain by a basal conglomerate passing upward into a sandstone unit and an overlying *Globotruncana*-bearing limestone (Okay et al., 2006). These relatively undeformed sedimentary rocks represent wedge-top basin deposits directly overlying the accretionary prism rocks (Festa et al., 2016). In other places, the Domuzdag complex is unconformably overlain by a lower-middle Eocene, nummulite-bearing neritic limestone unit (Okay et al., 2006).

Tectonically underlying the Domuzdag complex to the south is the thrust-imbricated Kargi Complex, which consists of garnet-amphibolite, garnet-mica schist and recrystallized limestone in its structurally upper section, and quartz-mica schist, quartzite, phyllite, and recrystallized limestone in its structurally lower section (Okay et al., 2006). These lower grade metamorphic rocks of the Kargi Complex are locally stratigraphically overlain by a <1-km-thick sedimentary assemblage, composed of *Globotruncana*-bearing micritic limestone, shale with sandstone clasts and blocks, conglomerate, debris-flow deposits, radiolarian chert, and blocks of gabbro and serpentinite (Kirazbasi Formation). We interpret the Kargi Complex as the tectonically lowest, thrust-imbricated unit of the subduction accretion system with the locally developed wedge-top basin deposits (Kirazbasi Formation) at the active margin of southern Eurasia (Fig. 2; this study).

KÜRE OPHIOLITE

Previous Studies and Interpretations

Previous studies of the Küre ophiolite have mainly focused on the occurrence of volcanogenic massive sulfide deposits and their origin (Kovenko, 1944; Güner, 1980; Nakayama and Kaya, 1999; Kusçu and Erler, 2002). The ophiolite and its sedimentary cover were first defined by Ustaömer and Robertson (1994) within the framework of the Paleotethyan tectonics of the Central Pontides; they interpreted the ophiolite and sedimentary cover as a 20-km-thick imbricate thrust package of oceanic rocks that originated from a late Paleozoic marginal basin along the southern edge of Eurasia. Ustaömer and Robertson (1994) correctly surmised that the Küre ophiolite was not associated with any Paleotethyan suture zone in the region, although the thickness of the ophiolite–sedimentary cover assemblage and the role of imbricate thrusting within the ophiolitic basement were overestimated in their study. Çakir et al. (2006) reported the occurrence and the mineral and whole-rock chemistry of lherzolitic intrusions within the crustal units of the Küre ophiolite; they interpreted these rocks as subduction-influenced, Mg-rich late-stage intrusions that were emplaced into a preexisting oceanic lithosphere of a marginal sea.

Igneous Stratigraphy of the Küre Ophiolite

The Küre ophiolite has a Penrose-type oceanic crust (Dilek, 2003b), complete with a sheeted dike complex (Fig. 3), and consists of upper mantle peridotites, ultramafic cumulates, layered to isotropic gabbros, sheeted dikes, and an extrusive sequence. The upper mantle peridotites consist mainly of harzburgite with dunite and minor lherzolite. There are no dike intrusions or rodingites within these peridotite units, as commonly reported from other suprasubduction zone Tethyan ophiolites in the eastern Mediterranean region (Dilek et al., 1999; Çelik and Delaloye, 2003). Dunite veins and layers increase in abundance in the upper parts of the harzburgitic peridotites and locally contain trace amounts of chromitite. Near the top of the upper mantle section dunite becomes rich in plagioclase and clinopyroxene, and includes lenses of clinopyroxenite and podiform chromitite layers.

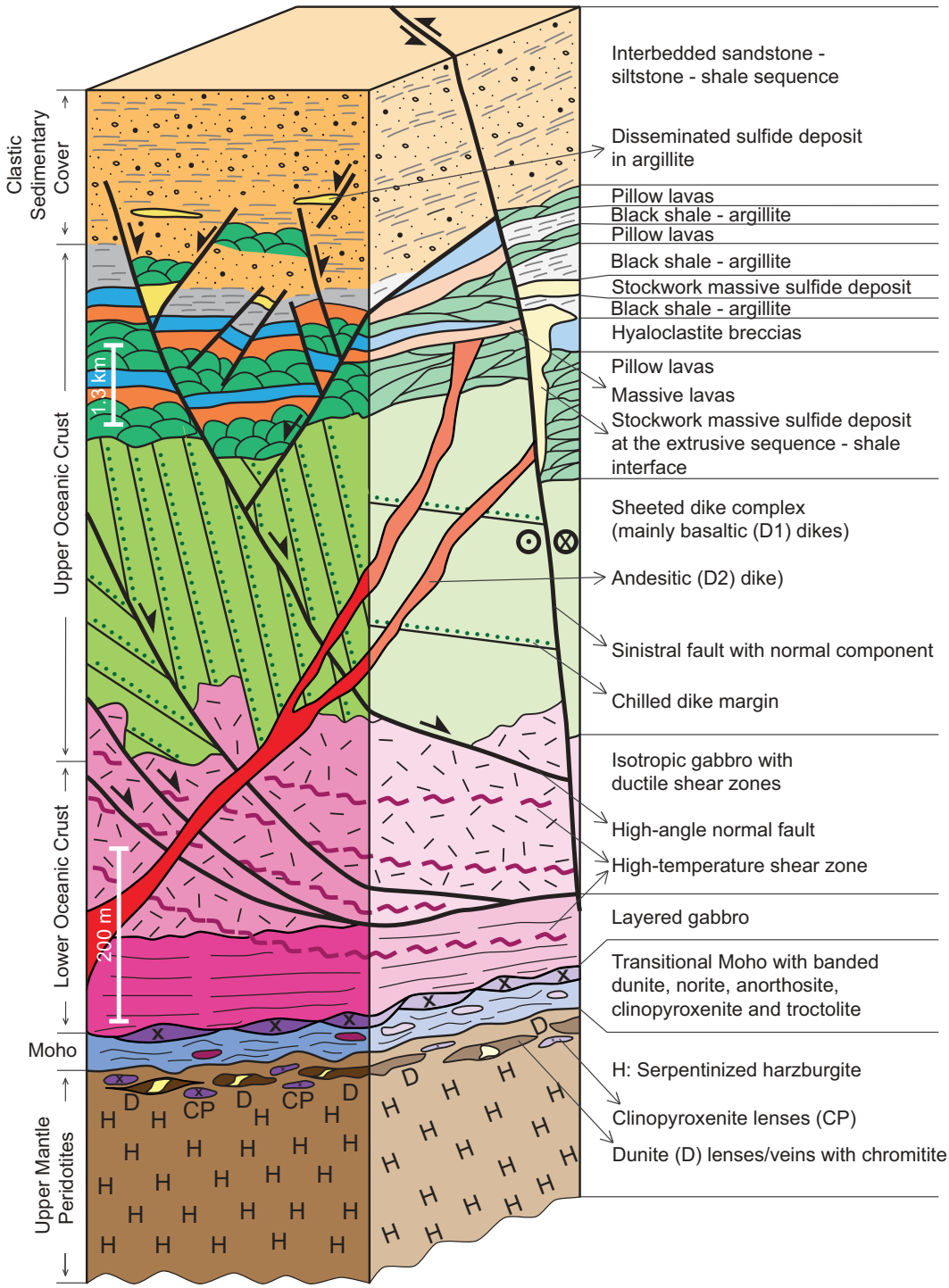

Figure 3. Synthetic three-dimensional lithostratigraphy and internal structure of the Küre ophiolite and its sedimentary cover (based on this study). Further discussion in the text.

The upper mantle peridotites are gradational upward into banded dunite interlayered with norite, troctolite, and anorthosite within an ~100-m-thick transitional zone with the overlying cumulate gabbros (Fig. 3). Layering in the cumulate gabbros is represented by alternating bands of clinopyroxene and anorthitic plagioclase that dip gently (30°–45°) to the south. The cumulate gabbros, ~150 m in thickness, are transitional upward into isotropic gabbros, which are locally cut by dolerite dikes (Fig. 4A) and wehrlite and lherzolite intrusions. Medium- to fine-grained isotropic gabbros are crosscut by brittle normal faults and ductile shear zones (locally 10 cm in width).

Sheeted dike swarms overlie the isotropic gabbros (Fig. 3) and form tabular intrusions ranging in width from 80 cm to 2 m (Fig. 5A) and displaying one- and two-sided chilled margins. The majority of the sheeted dikes are represented by northwest-striking doleritic dikes (in the present coordinate system), which make up the earliest dike generation (D1) (Fig. 5A). These doleritic dikes are crosscut by basaltic andesite and andesite dikes that constitute D2 and younger dike generations, most of which have northeast-southwest strikes (Figs. 5B, 5C). The northwest-southeast–oriented sheeted dikes are crosscut by dike-parallel, moderately to steeply dipping (both to the southwest and to the northeast) normal faults, and by northeast-southwest–striking and steeply northwest- or southeast-dipping oblique-slip faults.

The sheeted dike complex is overlain by an extrusive sequence composed of pillow and massive lava flows, pillow breccias, and hyaloclastites (Fig. 3). Pillow lava flows are consistently oriented approximately east-northeast–west-southwest with their convex-up tops commonly facing south (Fig. 6). Pillow lava flows have long-axis diameters of 20–30 cm (minipillows) to 1–2 m (megapillows). They have dark and glassy margins, moderately vesicular textures, and olivine-plagioclase phyric centers. Megapillows commonly occur at the bottom of an eruptive unit and grade upward into medium to minipillows, which are overlain by pillow breccias. Discrete eruptive units are separated by massive lava flows and hyaloclastite breccias (brecciate volcanic glass), which range in thickness from 50–80 cm to 5–6 m (Fig. 6). These massive lava flows and hyaloclastite breccias are commonly extensively altered and chloritized due to seafloor alteration. Massive lavas show fine-grained, chilled upper margins commonly facing south and coarse-grained centers. Hyaloclastite breccias exhibit crude bedding generally dipping to the south at moderate to steep angles (Fig. 6).

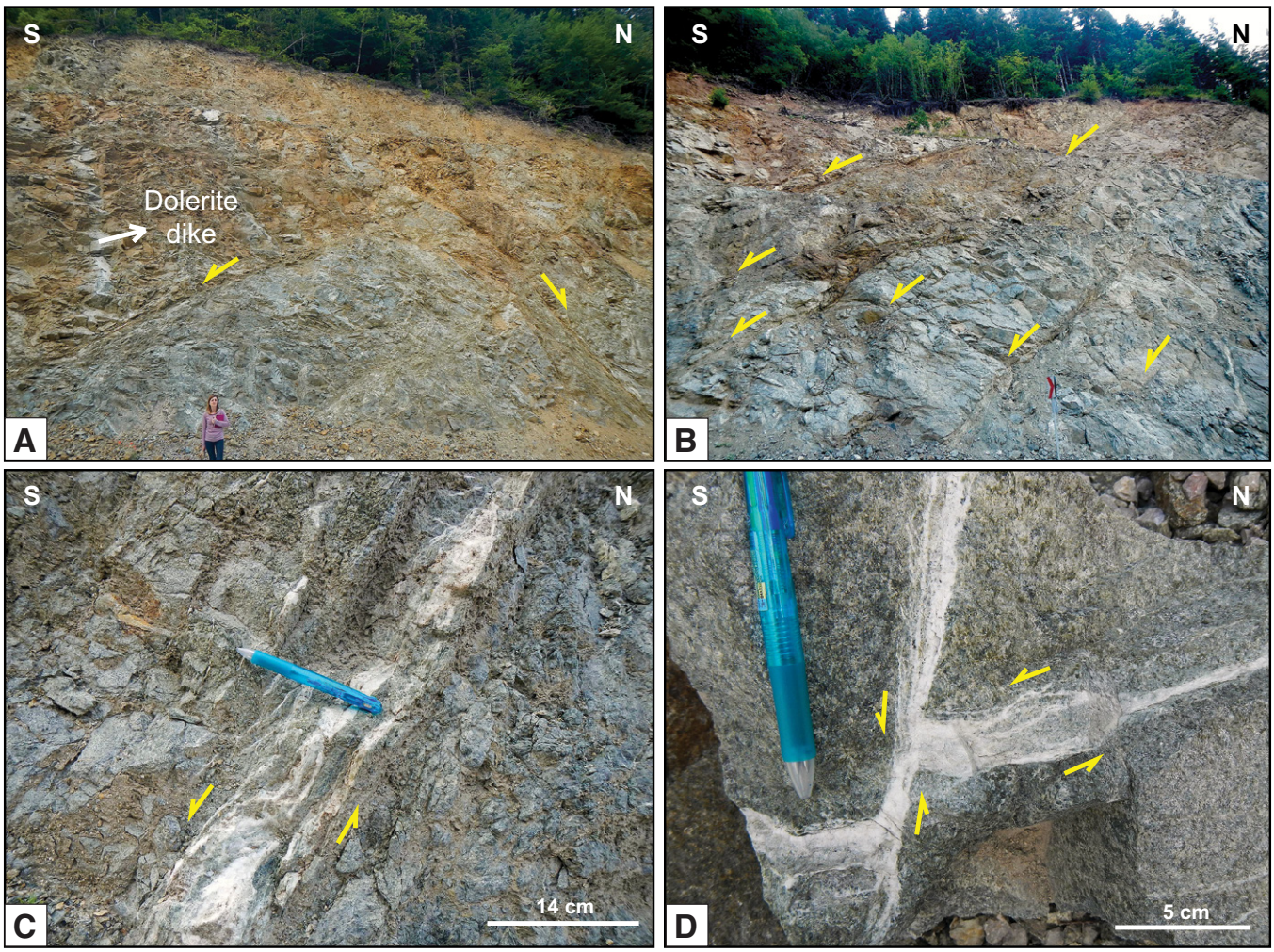

Figure 4. (A, B) Isotropic gabbros with brittle shear zones and faults. (C, D) Layered gabbros with ductile shear zones and faults. All extensional normal faults and shear zones display top-to-the-south shearing. An ~80-cm-thick dolerite dike in the isotropic gabbro (A) is truncated by a south-dipping, low-angle normal fault. A low-angle ductile shear zone containing mylonitized albite-quartz-epidote-chlorite veins is cut and displaced by a steeply dipping, younger shear zone with a similar mineral assemblage (D).

Pillow and massive lava flows and hyaloclastite breccias are locally extensively altered along northwest–southeast–striking oblique-normal fault systems and at the intersections of these faults with northeast-southwest–oriented strike-slip faults. These alteration zones can be several tens to several hundreds of meters wide. One of the largest fault-bound alteration zones is exposed near the town of Küre, where a stockwork volcanogenic massive sulfide deposit with pyrite, chalcopyrite, bornite, sphalerite, and marcasite mineralization occurs within the pillow lava–hyaloclastite–argillite intercalation (Fig. 7).

Sedimentary Cover of the Küre Ophiolite

Pillow and massive lava flows and pillow breccias in the top section of the Küre extrusive sequence are depositionally overlain by and intercalated with black argillite and shale-siltstone-sandstone layers. The contacts between the lava flows and the argillite and shale units are locally reactivated as normal faults (Fig. 7). Blocks of pillow breccia and hyaloclastites occur in the bottom section of the argillite and shale sequence. Siltstone and thinly bedded sandstone layers are rare in this bottom section, but become more abundant upsection in the sedimentary cover, where they form 5–7-m-thick sequences with thin, finely laminated shale interlayers. Sandstones have average bed thicknesses of 10–15 cm, and show graded bedding and lamination. Rare flute and groove casts in these sandstones indicate dominantly west-northwest–east-southeast paleocurrent directions. Sandstones contain subangular to angular clasts of quartz, feldspar, plagioclase, biotite, and schist in a silty or muddy matrix, and are poorly sorted. These features of the Küre sedimentary cover differ significantly from those of pelagic sedimentary cover lithologies of other Tethyan ophiolites (i.e., Troodos, Cyprus, Dilek and Eddy, 1992; Vourinos, Greece, Rassios and Dilek, 2008; Mirdita, Albania, Dilek et al., 2008; Kizildag, Turkey, Dilek and Thy, 1998), which consist mainly of chert, micritic limestone, and/or chalk deposits. However, the argillite and shale-sandstone- siltstone composition of the Küre sedimentary cover is similar to that of the Jurassic Josephine ophiolite (Galice Formation, northern California), which has been interpreted as fossil backarc basin oceanic lithosphere (Harper et al., 1994).

The sedimentary cover of the Küre ophiolite has been named the Akgöl Formation (Altun et al., 1990). The stratigraphically uppermost level of the formation contains limestone blocks with a basal conglomerate (Ustaömer and Robertson, 1994; Okay et al., 2014). Limited foraminifera fossils obtained from these limestone blocks have revealed Middle–Late Triassic to Early Jurassic ages (Altun et al., 1990), and few trace fossils have provided a Late Triassic age (Kozur et al., 2000). The Küre ophiolite and its sedimentary cover are cut by dikes, stocks, and plutons of the Middle Jurassic Kastamonu granitoid belt (Altun et al., 1990; Boztug et al., 1984). The entire ophiolite–sedimentary cover sequence and the Kastamonu granitoid plutons in the region are unconformably overlain by an upper Jurassic–lower Cretaceous basal conglomerate and shallow-water carbonates (Altun et al., 1990; Ustaömer and Robertson, 1994).

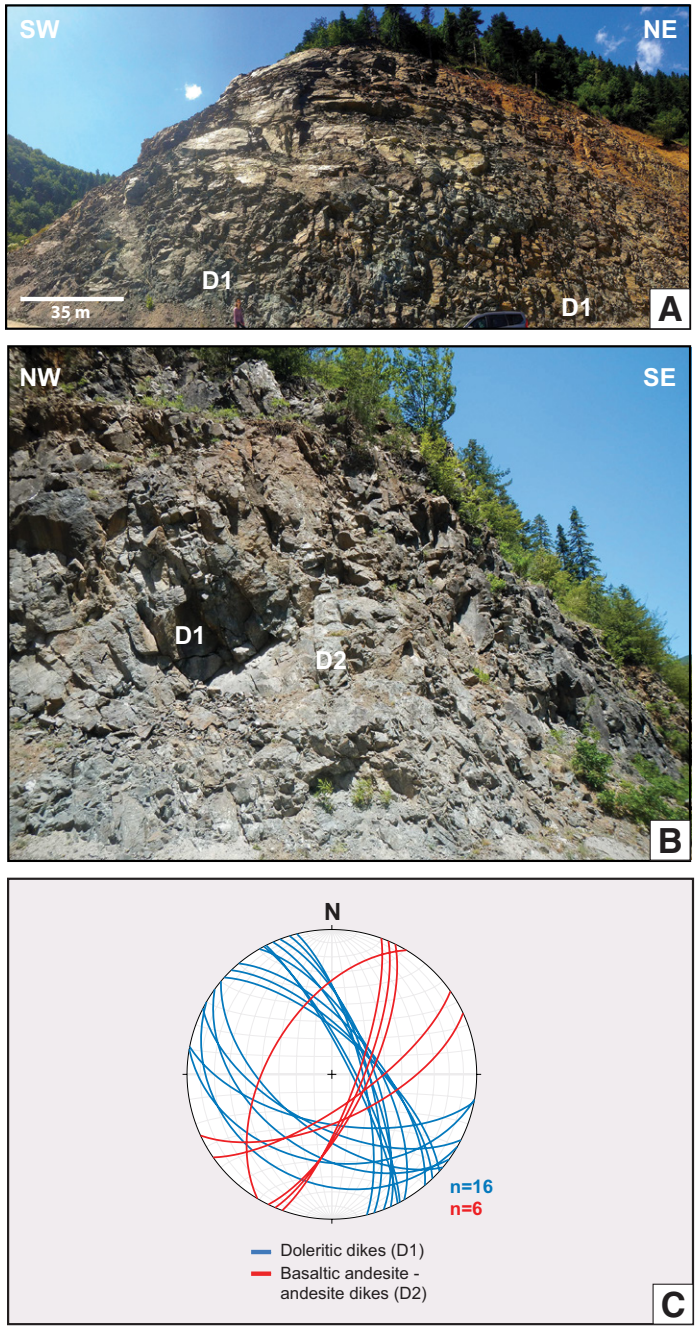

Figure 5. Tabular dike intrusions in the Küre sheeted dike complex. (A) Northwest-southeast–oriented doleritic dike swarms (D1 generation), which make up the majority of the dike complex. View is to the northwest. (B) Northwest-southeast–oriented sheeted dolerite dikes are crosscut by a northwest-southeast–striking andesitic dike (D2). View is to the northeast. (C) Lower hemisphere equal area stereonet plot of representative dike intrusions and generations in the sheeted dike complex.

STRUCTURAL ARCHITECTURE OF THE KÜRE OPHIOLITE AND ITS SEDIMENTARY COVER

The crustal units of the ophiolite and the clastic sequence overlying them display widespread extensional and contractional deformation structures that developed during the seafloor spreading evolution of the ocean basin and its subsequent closure stages. Most of the normal fault systems in the sheeted dike complex and within the extrusive sequence are spatially and temporally associated with hydrothermal mineralization and alteration zones. Some normal faults in the extrusive sequence are overlain by younger lava flows. These features indicate that the observed extensional faults formed synchronously with active magmatism during oceanic crust generation. Contractional deformation structures are represented by several different foliation types, folds, and reverse-thrust faults that are manifested best in the clastic sedimentary cover rocks.

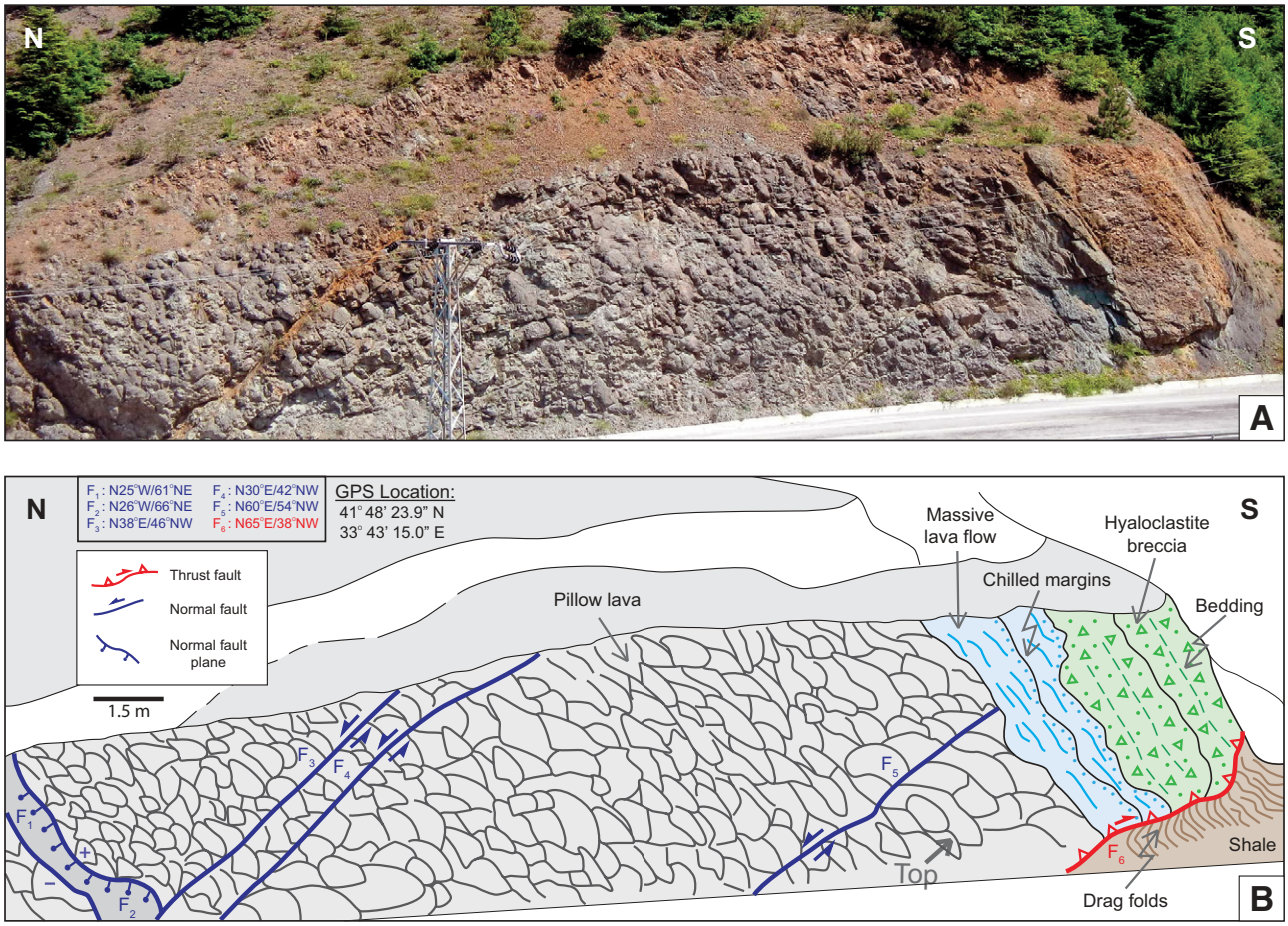

Figure 6. A typical profile of the extrusive sequence of the Küre ophiolite, showing the pillow lava, massive lava, and hyaloclastite breccia units with a younging direction to the south. (A) Outcrop photo. (B) Interpreted image based on field observations and measurements. The massive lava flows, with their chilled margins, and the overlying, bedded hyaloclastite breccias dip steeply to the south, and stratigraphically overlie the normal-faulted pillow lava flows. The extrusive sequence units in this outcrop are thrust southward over the black shale of the sedimentary cover of the ophiolite. F—fault; GPS—global positioning system.

Record of Extensional Deformation

The layered and isotropic gabbros in the lower crustal part of the ophiolite display ductile and brittle shear zones and normal faults (Fig. 4). Brittle normal faults form two subsets, based on their orientations: nearly east-west–striking and moderately to steeply (40°–60°) north- and south-dipping faults, and northwest-southeast–striking faults with gentle to moderate southwest dip angles (20°–40°) (Fig. 8A). The faults in the latter group have anastomosing patterns in the outcrop with a fault interval of 2–5 m, forming fault zones with lozenge-shaped blocks of highly fractured gabbroic rocks showing kinematic indicators of top-to-the-south shearing (Figs. 4A, 4B). These fault zones are commonly associated with albite-quartz-chlorite-epidote-actinolite ± hornblende veins, which commonly form as a result of channelized fluid flux (with a temperature range of 300–700 °C; McCollom and Shock, 1998) along fault planes in the oceanic lower crust (Coogan et al., 2006). Ductile shear zones range in width from several centimeters to 20 cm, are moderately to steeply dipping, and include mylonitized gabbroic rocks exhibiting consistently top-to-the-south shear indicators (Figs. 4C, 4D).

Dike swarms in the sheeted dike complex show two major clusters in their orientations. The majority of the sheeted dikes are composed of medium-grained doleritic dikes, which constitute the first dike generation (D1). A subset of these D1 dikes strike northwest–southeast and dip steeply (65°–80°) northeast (Fig. 5C). Another subset of D1 dikes strikes west-northwest–east-southeast and dip gently to moderately (20°–50°) southwest (Fig. 5C). These orientations of the D1 dikes suggest a north-northeast–south-southwest direction of extension during the seafloor spreading formation of the Küre oceanic crust. D1 dikes are intruded by D2 generation younger basaltic andesite and andesite dikes that strike northeast-southwest and dip steeply (65°–76°) to the southeast (Fig. 5C).

The sheeted dikes are crosscut by northwest–southeast–extending normal faults and by east-northeast–west-southwest–striking oblique-slip faults (Fig. 8B). The northwest–southeast–oriented normal faults are subparallel to the D1 sheeted dikes, and dip either steeply (65°–80°) to the northeast or gently (15°–40°) to the southwest (Fig. 8B). The high-angle, northwest–southeast–striking normal faults are commonly associated with quartz-epidote-hematite mineralization within hydrothermal alteration zones that are several millimeters to 10–15 cm wide. The east-northeast–west-southwest–extending oblique-slip faults dip steeply (60°–86°) to the northwest or southeast (Fig. 8B). These subvertical oblique-slip fault planes contain subhorizontal to gently plunging (10°–15°) slickenside lineations, marked by the preferred alignment of chlorite-quartz-calcite mineral growth.

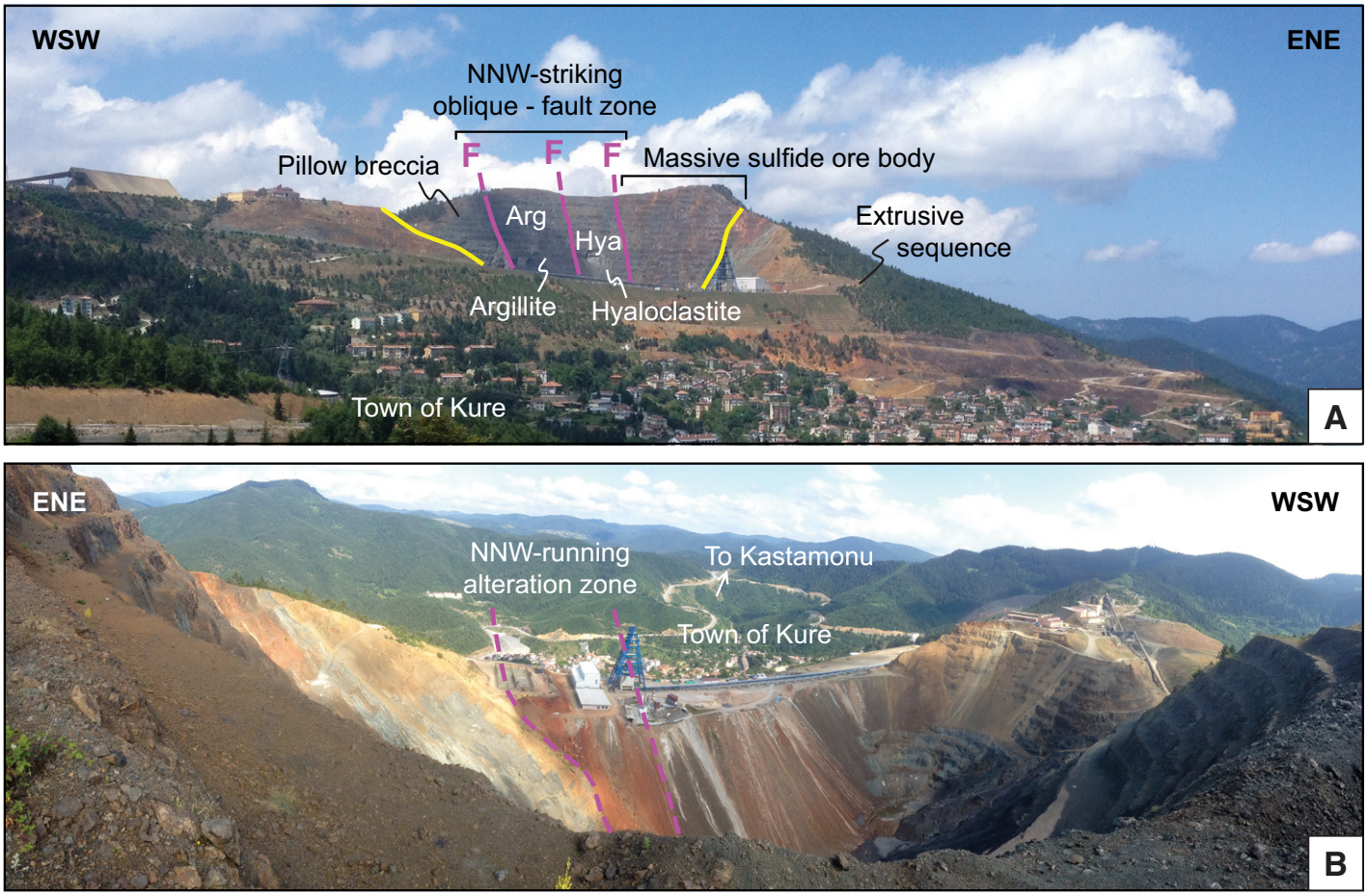

Figure 7. Panoramic views of the active massive sulfide deposit mine in Küre. (A) North side. (B) South side. The deposit forms a conical mound largely situated within the extrusive sequence of the ophiolite and adjacent to a north-northwest–southeast–oriented left-lateral oblique-normal fault zone. This fault zone continues to the southeast as a major alteration zone, in which all extrusive rocks are hydrothermally leached.

The extrusive sequence is extensively faulted, which resulted in hydrothermal mineralization and horizontal axis rotation of both pillow and massive lava flows (Figs. 6 and 9). Some of the normal faults are overlain by undisturbed lava flows, indicating that extensional faulting was episodic and that it was followed by renewed phases of volcanism (Fig. 6). There are two major normal fault groups observed in the extrusive sequence, based on their orientations: northwest–southeast–striking and southwest-northeast–dipping faults, and northeast-southwest–oriented and southeast- and northwest-dipping faults (Figs. 8C, 8D). Dip angles of the both groups range from 10° to 80°. These faults commonly display quartz-epidote-hematite mineralization effects and vertical to subvertical slickenside lineations. In addition to these normal faults, the extrusive rocks are also crosscut by northwest-southeast– and northeast-southwest–striking and steeply dipping oblique-slip faults with normal components. These faults exhibit moderately plunging (40°–65°) slickenside lineations on the fault planes.

The majority of the northwest-southeast–striking normal faults dip to the southwest at low angles (10°–45°) and display listric geometries with depth (Figs. 9 and 10). They crosscut and displace earlier formed normal faults; some younger synthetic faults in the extrusive rocks sole out at these low-angle listric normal faults (Fig. 10). These low-angle normal faults locally display several-meters-wide cataclastic shear zones, which include mechanically disintegrated and intensely fractured slivers of lava rock in a medium- to fine-grained and brecciated matrix (Fig. 11). These cataclastic shear zones consistently show kinematic indicators for extensional simple shear deformation.

The argillite and sandstone-siltstone-shale sequence in the sedimentary cover of the ophiolite was also affected by extensional deformation and normal faulting (Fig. 9). Almost all the observed normal faults in the sedimentary cover are northwest-southeast oriented, with moderate to steep dips (50°–75°) to the northeast or southwest (Fig. 8E).

Contractional Deformation in the Sedimentary Cover

The argillite and sandstone-siltstone-shale sequence displays well-developed bedding that has a strong northeast-southwest attitude (Fig. 12A). The bimodal distribution of the bedding dip angles in the two maxima in Figure 12A is a result of folding (discussed herein), with steeply southeast-dipping (55°–85°) and moderately to gently northwest-dipping (7°–45°) layers. Bedding-parallel foliation is well developed in clay-rich argillite and shale interlayers, and mimics the bimodal bedding-plane orientations (Fig. 12B). The bedding-parallel foliation in the shale was likely a result of a smectite to illite phase change in clay mineralogy due to burial diagenesis (Lanson et al., 2009), followed by flattening strain.

The clastic rocks in the cover sequence are folded intensely, forming tight to isoclinal folds, best displayed by the competent sandstone layers

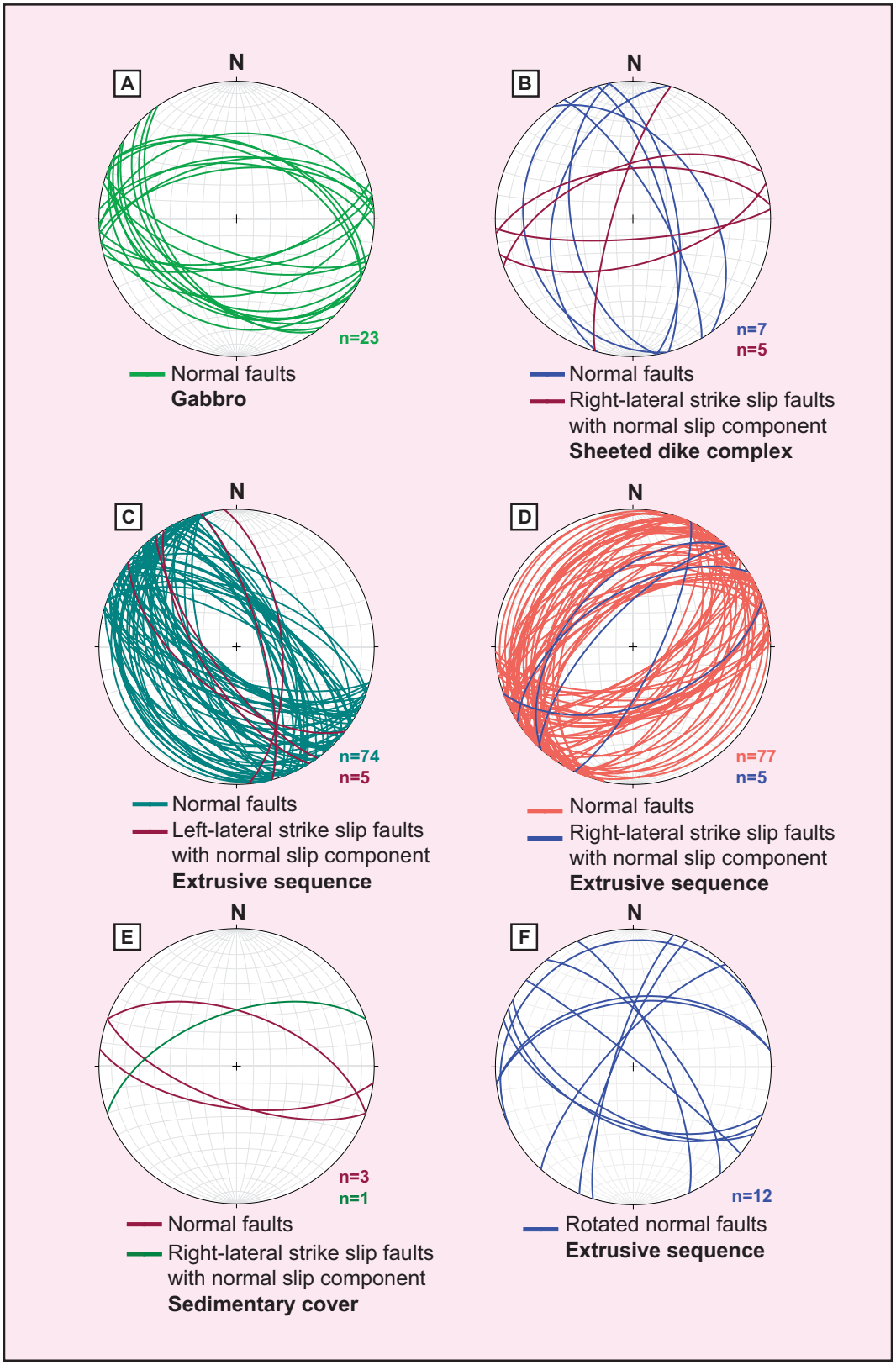

Figure 8. Lower hemisphere, equal area stereoplots of the measured normal and oblique-slip fault systems in the ophiolitic subunits and in the sedimentary cover. See text for discussion.

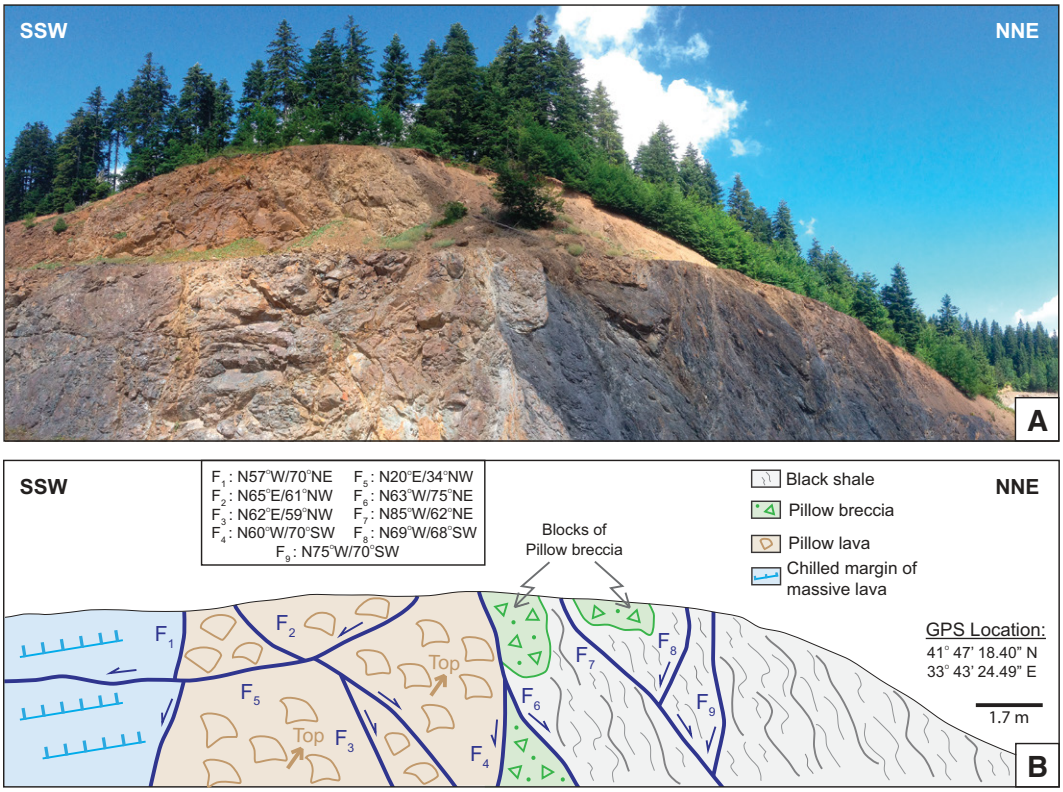

Figure 9. The extrusive sequence–sedimentary cover relationships at the bottom of the clastic rock units. Normal-faulted pillow lava flows are overlain by pillow breccias and fine-grained black shale, but the original contacts are superposed by later stage, north-northeast–south-southwest–dipping conjugate normal fault systems. Blocks of pillow breccia occur in the black shale as olistoliths. (A) Outcrop photo. (B) Interpreted image based on field observations and measurements. F—fault; GPS—global positioning system.

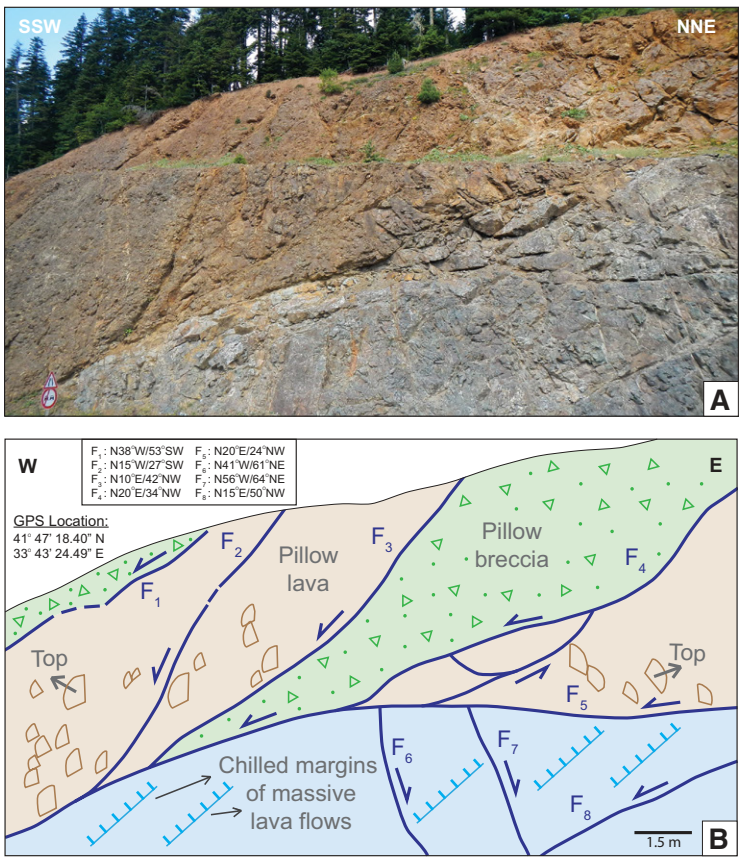

Figure 10. Crosscutting extensional normal fault geometries within the upper part of the Küre extrusive sequence. Thick massive lava flows that are cut across by high-angle normal faults are truncated by a northwest-dipping, low-angle (24°) fault displacing the pillow lava and pillow breccia units in its hanging wall. Pillow lavas are rotated into near subvertical orientations along moderately dipping, normal faults, which sole into the low-angle normal fault. (A) Outcrop photo. (B) Interpreted image based on field observations and measurements. F—fault; GPS—global positioning system.

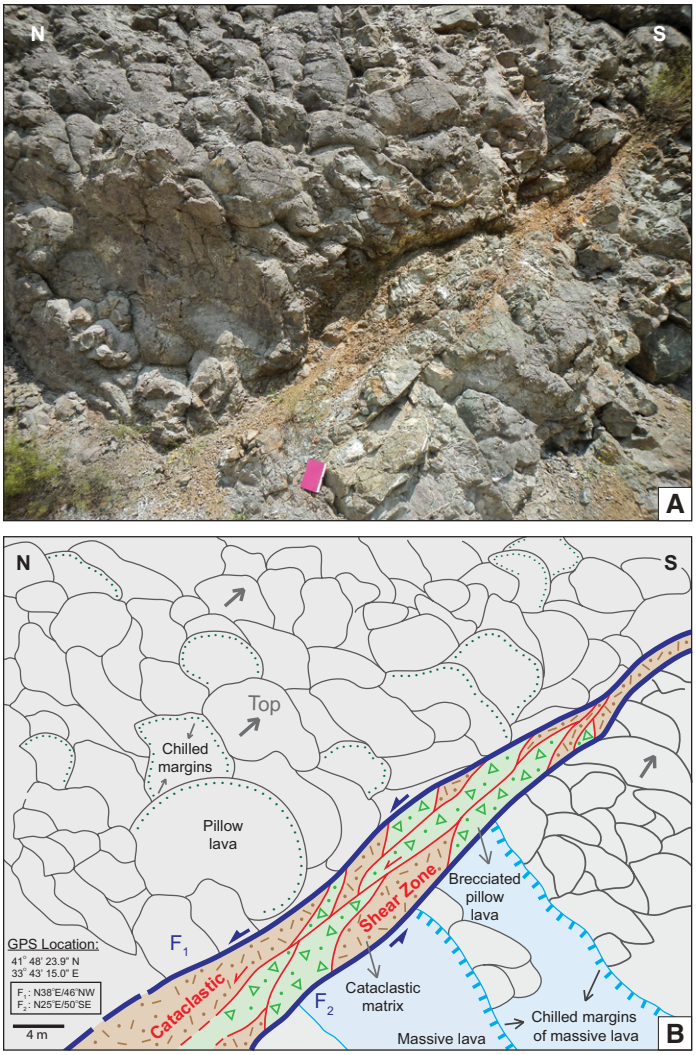

Figure 11. A 2–6-m-wide cataclastic shear zone, dipping moderately (40°–45°) to the north and truncating two massive lava flows at high angles. Pillow lava flows are rotated into this shear zone and are facing south. Highly brecciated pillow lava rocks within the shear zone are cut by anastomosing microfaults that display top-to-the-north shearing. (A) Outcrop photo. (B) Interpreted image based on field observations and measurements. F—fault; GPS—global positioning system.

(Fig. 13). The majority of the folds in the sandstone-siltstone units are parallel folds with intercalated shale layers, which show extreme attenuation on the fold limbs and thickening of their hinge zones (Figs. 13A, 13B). Most folds are highly asymmetric, with short and steeply dipping limbs overturned to the south (Fig. 11B). The fold axes plunge gently to moderately east-northeast (Fig. 12C). Drag folds and fault-propagation folds spatially associated with reverse and thrust faults are also common in the cover sequence.

Much of the contractional shortening in the sedimentary cover units was taken up by reverse and thrust faulting (Fig. 12D), which caused imbricate stacking, shearing of bedding planes, and development of a broken formation (Fig. 14). The observed reverse and thrust faults strike northeast-southwest or east-northeast–west-southwest, and their vergence is to the southeast or northwest (Fig. 12D). The shale-sandstone turbiditic sequence is locally deformed by anastomosing and subparallel reverse-thrust faults, which developed duplex structures, intrafolial folds, and floating fold noses in a shaly matrix, and highly attenuated and folded sandstone blocks in an intensely foliated shale matrix (Fig. 14). These structures are collectively analogous to those observed in sedimentary mélanges and broken formations that are documented to have developed at shallow depths in accretionary prisms and in foreland fold and thrust belts (Cowan, 1985; Festa et al., 2010; Yamamato et al., 2011). In one outcrop (41°48′26″N, 33°43′17.5″E), a broken formation tectonically overlies a relatively intact sandstone and shale sequence along a low-angle (26°), northwest-vergent thrust fault, which shows a well-developed flat-ramp geometry along the sandstone-shale interface (Fig. 14). The previously formed extensional normal faults in its footwall were truncated by this younger low-angle thrust fault. A similar broken formation in the sedimentary cover is exposed farther north (41°50′26.6″N, 33°42′38.6″E), where elongated, facoidal lenses and/or lozenges of siltstone occur in an argillite matrix, which displays a strongly developed anastomosing braided foliation and intrafolial folds (Fig. 15). Shear sense indicators in this outcrop show top-to-the-south-southwest contractional simple shear deformation.

Locally within the sedimentary cover the extrusive sequence of the ophiolite is also involved in south-vergent, thin-skinned thrust faulting. Near the town of Küre (41°48′23.9″N, 33°43′15.0″E) a nearly 30-m-thick pillow and massive lava and hyaloclastite breccia volcanic sequence is thrust over the shale unit (Fig. 6). Drag folds in the black shale in the footwall of the northeast-striking and gently (38°) northwest-dipping thrust fault provide strong evidence for southeast-directed tectonic transport and shortening in the oceanic basin of the ophiolite.

GEOCHRONOLOGY

In order to constrain the igneous age of the Küre ophiolite and the sources and the possible ages of detrital material within the sedimentary cover of the ophiolite, the U-Pb laser ablation–inductively coupled plasma–mass spectrometry (LA-ICP-MS) zircon dating method was used in this study. One sample (31-K-15) was collected for U-Pb zircon analysis from a gabbro in the Küre ophiolite and one sample (05-K-15) for detrital zircon analysis from a turbiditic sandstone in the sedimentary cover. We hand-picked 55 grains of magmatic zircons under a binocular microscope from the gabbro sample and 100 detrital zircon grains from the sandstone sample. U-Pb zircon measurements were done by LA-ICP-MS at the Key Laboratory of Crust-Mantle Materials and Environments Chinese Academy of Sciences, University of Science and Technology of China (Hefei, Anhui). The zircon grains were ablated with a 32 μm laser-spot diameter, 50 s (90 s in total) laser ablation time, and zircon 91500 adopted as an external standard for U-Pb dating. The ablated material was transferred from a closed cell in a helium carrier gas to an ICP-MS for laser ablation. The data were corrected by using an Excel spreadsheet of ComPbCorr#3-18 and age calculation was done with the program LaDating@Zn Excel VBA Program (Andersen, 2002) (Tables DR1 and DR2 containing the zircon data are provided in the GSA Data Repository[1]).

Gabbro sample 31-K-15 (41°50′20.2″N, 33°42′40.1″E) includes mainly euhedral zircon crystals with magmatic zoning (Fig. 16A). The analyses of the concordant data points give a Middle Jurassic crystallization age of the gabbro and an average $^{206}Pb/^{238}U$ age of 168.8 ± 2.0 Ma (Figs. 17A, 17B). We interpret this age as the timing of the oceanic crust formation in the Küre ocean basin.

[1]GSA Data Repository Item 2018054, Tables DR1 and DR2, U-Pb zircon age data from (1) gabbro and (2) sandstone samples from the Küre ophiolite, northern Turkey, is available at http://www.geosociety.org/datarepository/2018, or on request from editing@geosociety.org.

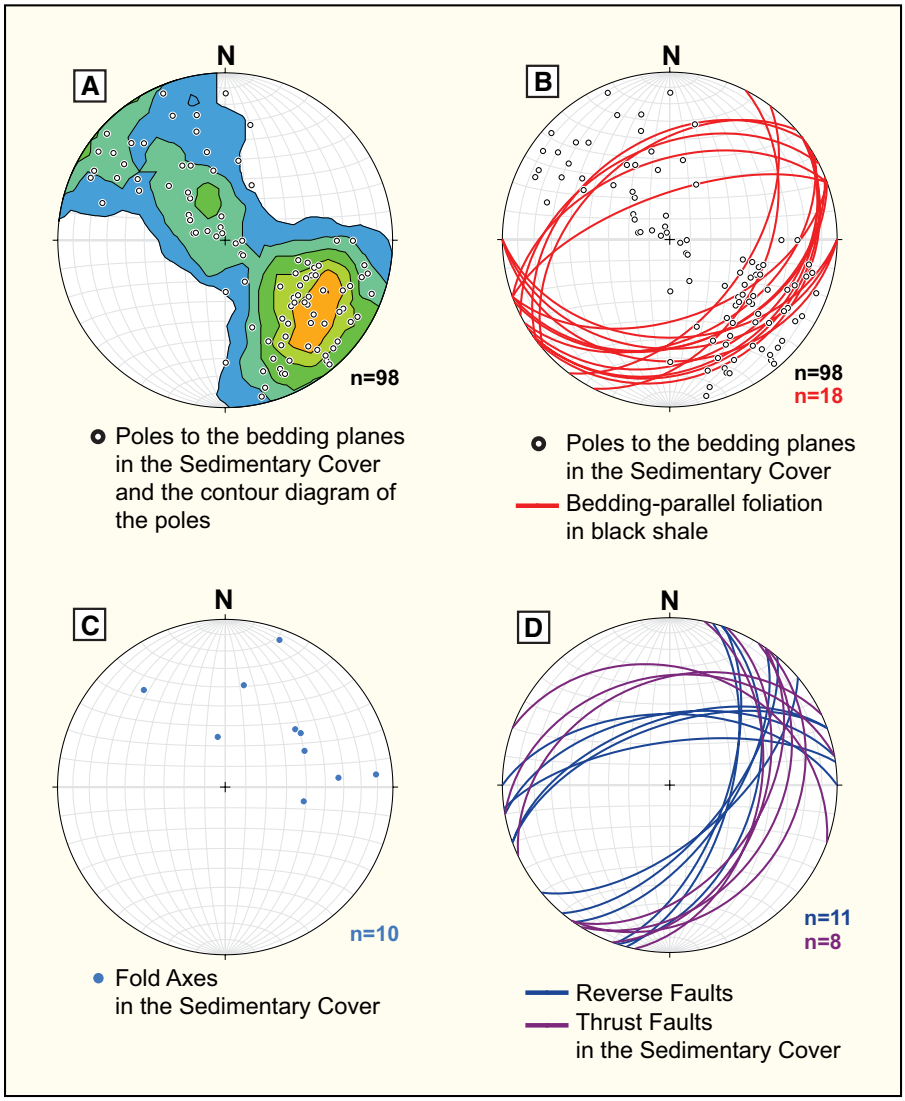

Figure 12. Lower hemisphere, equal area stereoplots of the primary and deformation fabric elements and structures in the sedimentary cover of the ophiolite. See text for further discussion.

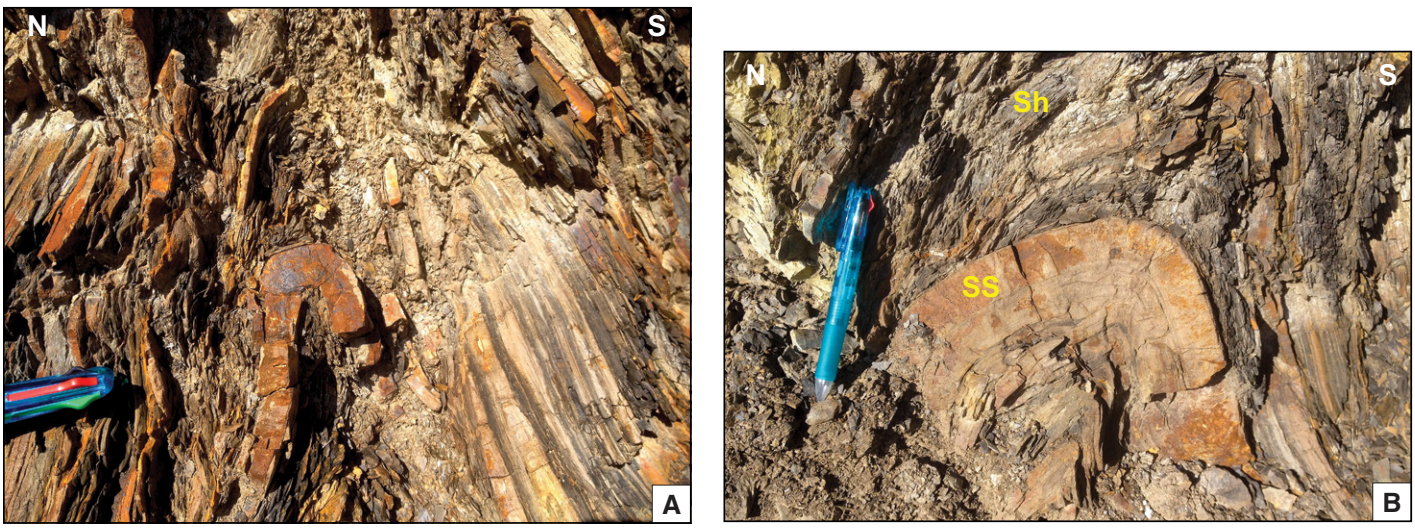

Figure 13. Isoclinal and nearly southward-overturned parallel folds in the sandstone (SS) and shale (Sh) interlayers in the sedimentary cover. The fold axes of the folds in this outcrop all plunge gently to the northeast.

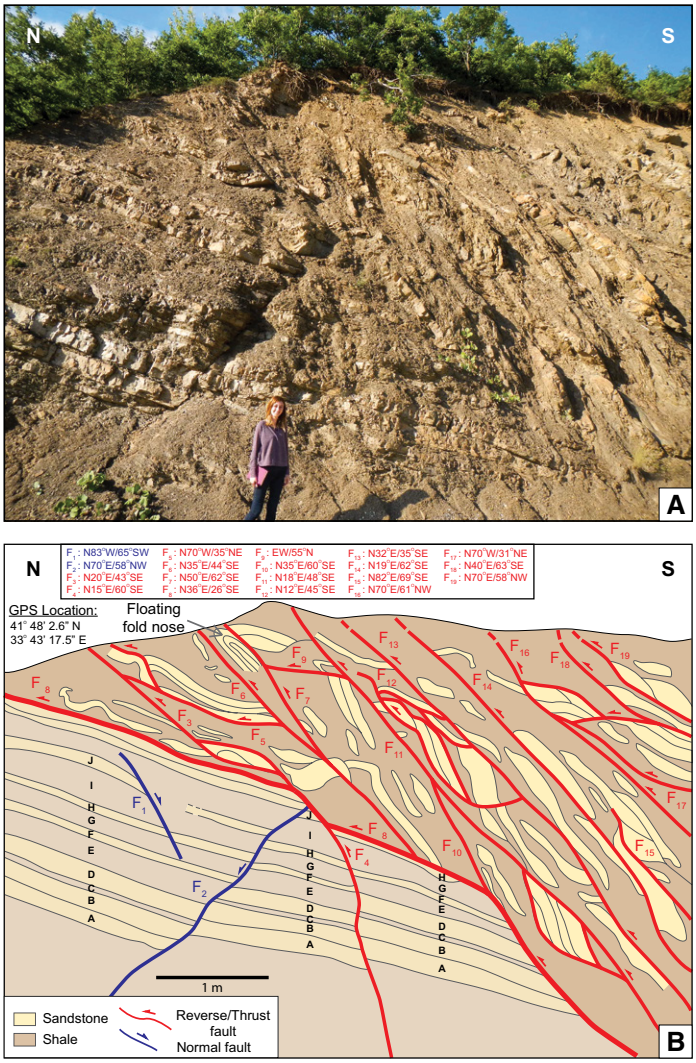

Figure 14. A north-vergent, low-angle (26°) thrust fault with a flat-ramp geometry, emplacing a broken formation with an incipient mélange character in its hanging wall over a relatively undeformed sandstone-siltstone-shale sequence in the footwall. (A) Outcrop photo. (B) Interpreted image based on field observations and measurements. F—fault; GPS—global positioning system. See text for further discussion.

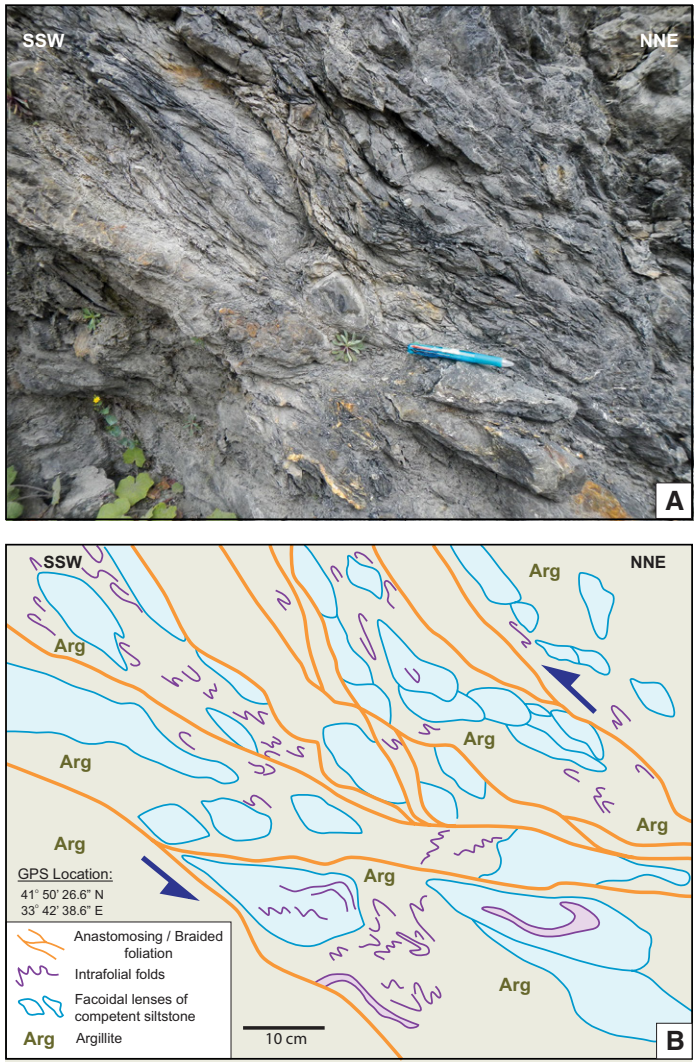

Figure 15. A broken formation with elongated, facoidal siltstone and sandstone lenses in an intensely sheared argillite matrix, which displays anastomosing foliation, intrafolial folds, and floating fold noses that collectively indicate top-to-the-south-southwest contractional shearing. (A) Outcrop photo. (B) Interpreted image based on field observations and measurements. F—fault; GPS—global positioning system.

Sandstone sample 05-K-15 (41°47′22.8″N, 33°43′25.0″E) contains euhedral zircon crystals and fragments (Fig. 16B). The probability density diagram of the obtained data shows a youngest $^{206}Pb/^{238}U$ age of 197 Ma and an oldest $^{206}Pb/^{238}U$ age of 2.8 Ga (Fig. 17C). The major detrital zircon age groups include Paleozoic and early-Late Triassic clusters; 26 zircon data points indicate Proterozoic ages and 3 zircon data points show $^{206}Pb/^{238}U$ ages of 3386 ± 124 Ma, 2715 ± 68 Ma, and 2683 ± 98 Ma (Fig. 17C). The analyses of 22 zircon ages reflect inherited Paleoproterozoic and Archean crustal components (Fig. 17C).

U-Pb analysis of detrital zircon age populations is used effectively to identify a potential provenance by matching detrital zircon ages with the crystallization ages of possible source rocks in a region (Thomas, 2011). The crystalline basement rocks in the Istanbul zone to the west and northwest of the Küre ophiolite have Eurasian tectonic affinities and include Paleozoic and Precambrian rock units, as in the Moesian and Scythian platforms in easternmost Europe and to the north of the Black Sea. These basement units once constituted the Laurasian continental margin (Okay, 2008). The Ukrainian shield, which is part of the East European Craton, makes up the tectonic basement of the Moesian and Scythian platforms and contains granite gneiss (3.65 Ga) and Paleoproterozoic crustal units (2.2–2.0 Ga) (Claesson et al., 2006).

The Kursk microcontinent, which makes up the crystalline basement of East Europe, contains 3.7–3.1 Ga metasedimentary and metavolcanic sequences forming a granite greenstone belt (Mints, 2015). The middle Paleoproterozoic tectonostratigraphic complexes of the Bryansk-Kursk-Voronezh collisional orogeny in East Europe include migmatized rocks of the Kulazhino Group (2.95–2.56 Ga), the Kursk Group (2.3–2.1 Ga), and the Oskol Formation (2.06–2.04 Ga). Granitoid intrusions in this orogenic belt range in age from 2.10 to 2.08 Ga in the Usman and Pavlovsk complexes, and from 2.08 to 2.05 Ga in the Mamon and Yelan complexes (Mints et al., 2015).

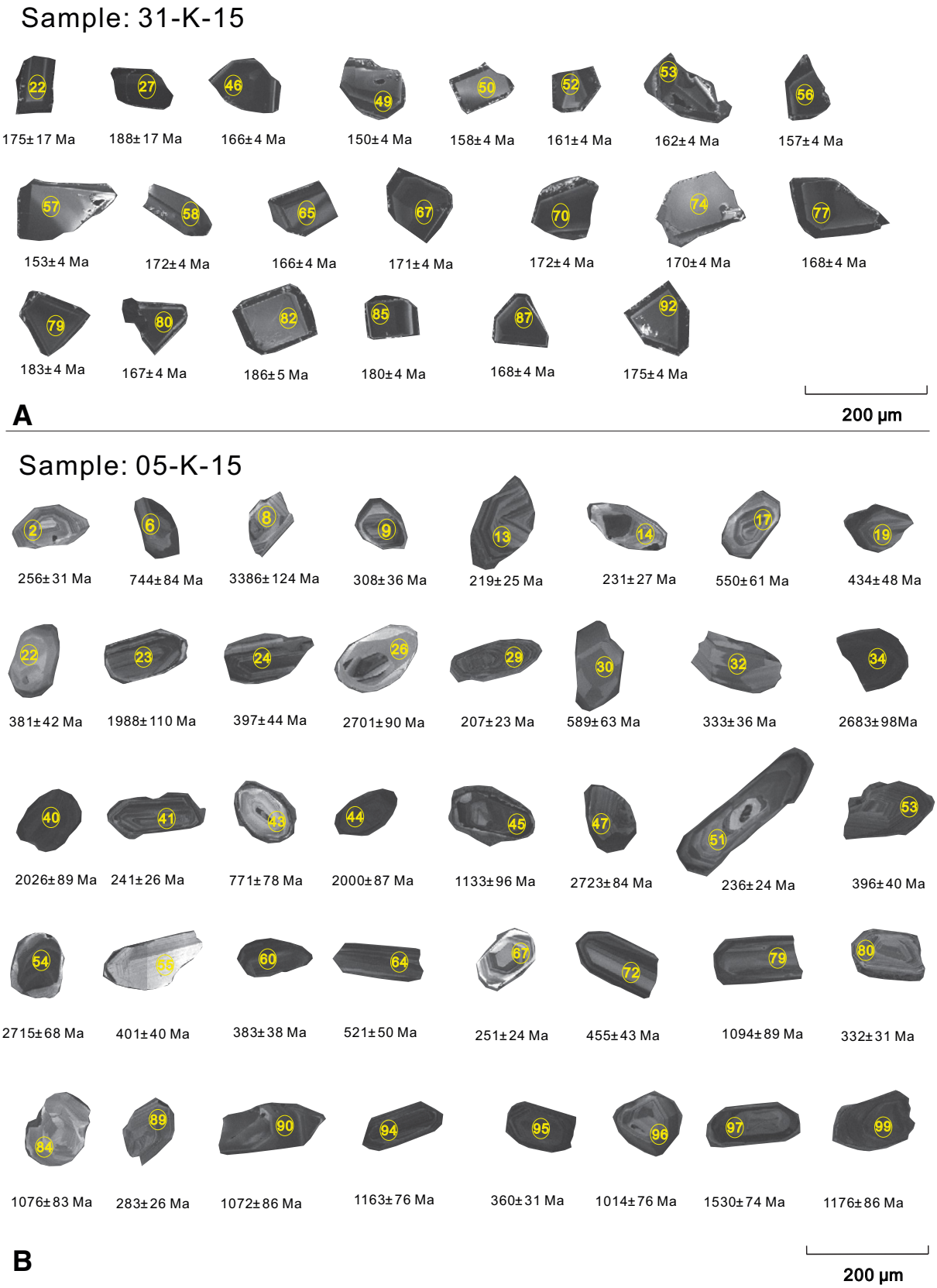

Figure 16. Cathodoluminescence images of representative zircon grains in the sedimentary cover of the ophiolite that are analyzed in this study. (A) From a gabbro sample (31-K-15). (B) From a sandstone unit (05-K-15) in the sedimentary cover of the ophiolite analyzed in this study.

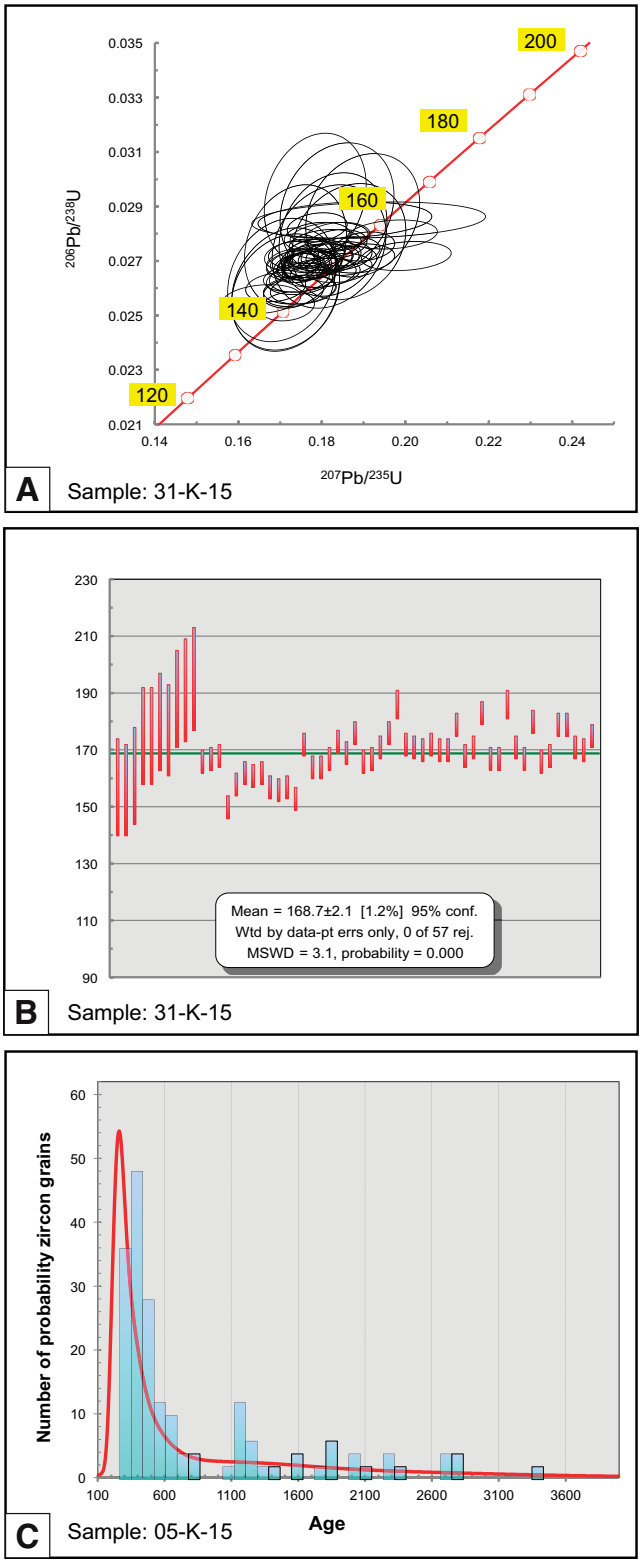

Figure 17. (A) Laser ablation–inductively coupled plasma–mass spectrometry (LA-ICP-MS) zircon U-Pb concordia diagram from Küre ophiolite gabbro sample 31-K-15. (B) Weighted (Wtd) average crystallization age of zircons from sample 31-K-15. Data-point error (data-pt err) symbols are 2σ (conf.—confidence; rej.—rejected). MSWD—mean square of weighted deviates. (C) Relative probability density plot for detrital zircon grains from a sandstone unit (sample 05-K-15) in the sedimentary cover of the Küre ophiolite.

Rocks of similar Precambrian ages do not occur in central and southern Anatolia (Okay, 2008). Therefore, the Archean and Paleoproterozoic detrital zircons recovered from the sedimentary cover of the Küre ophiolite in this study clearly indicate a northern source in the peri–Black Sea region, specifically in East Europe, at the time of the seafloor spreading and closure evolution of the Küre basin. This inference is consistent with the limited northwest to southeast paleocurrent directions observed in the turbiditic sandstones. Thus, the Küre basin appears to have developed as a continental backarc basin within the Eurasian realm in the Middle Jurassic.

TECTONIC EVOLUTION OF THE KÜRE OPHIOLITE

Continental Backarc Basin Origin of the Küre Ophiolite

Geochemical Constraints

We have analyzed representative samples of the pillow and massive lava flows, sheeted dikes, and isotropic gabbros from the Küre ophiolite to elucidate the geochemical affinities and isotopic signatures of their magmas. We present and discuss these geochemical and isotopic data and their interpretations in detail elsewhere. We summarize here the geochemical features of the Küre lavas and dikes to provide a geochemical perspective for our interpretation of the tectonic setting of formation of the Küre ophiolite. The majority of the lava and dike rocks have basalt and basaltic andesite and andesite compositions (Fig. 18A) with tholeiitic to calc-alkaline signatures. We have employed two widely used discrimination diagrams based on the elements Ti, V, Th, and Nb, which are considered most stable during metamorphism and alteration of basaltic rocks (Staudigel and Hart, 1983; Seyfried et al., 1988; Hofmann and Wilson, 2007; Dilek et al., 2008). These diagrams are therefore most likely to reflect the original magma compositions. The Küre extrusive and sheeted dike rocks plot in the slab-proximal backarc basin basalt (BABB) field on a Ti-V diagram (Shervais, 1982; Dilek and Furnes, 2014), and mainly in the BABB field (some dikes also plot in the island arc tholeiite, IAT, field) on a Th_N-Nb_N diagram (Figs. 18B, 18C; Saccani, 2015). On these two discrimination diagrams we also plotted some of the representative lava data from the Bransfield Strait, which represents a Quaternary ensialic backarc basin at the northern tip of the Antarctic Peninsula (Keller et al., 2002), and from the middle Miocene, ensialic Sea of Japan (Yamato subbasin) backarc basin in the northwest Pacific Ocean (Hirahara et al., 2015) for comparison (Figs. 18B, 18C). The Küre samples, together with the Bransfield and Yamato basin lavas, plot largely in the BABB field on the Th_N-Nb_N diagram, with some samples displaying normal (N) MORB to enriched MORB affinities. On a chondrite-normalized rare earth element (REE) concentration diagram (Fig. 18D) the Küre samples straddle the Lau Ridge and Lau Basin field (Ewart et al., 1998) and significantly overlap with the average N-MORB and BABB patterns. Collectively, these geochemical features and comparisons suggest that the Küre lavas and dikes display MORB- and IAT-like affinities with slight light (L) REE enrichment patterns, typical of backarc basin magmas (Keller et al., 2002; Hawkins, 1977, 2003; Stern and de Wit, 2003; Hirahara et al., 2015).

The regional geology of the Küre ophiolite within the Sakarya terrane is also consistent with this geochemical inference. The spatial and temporal distribution of the Çangaldag magmatic arc (172–161 Ma), the Elekdag forearc ophiolite, and the Kargi metamorphic complex (Early Cretaceous Domuzdag and Kargi subduction-accretion complexes to the south; Fig. 2) support a backarc basin origin of the Küre ophiolite.

Structural and Stratigraphic Constraints

The structural and geochronological data obtained in this study suggest that the paleo-oceanic crust exposed in the Küre ophiolite formed at a

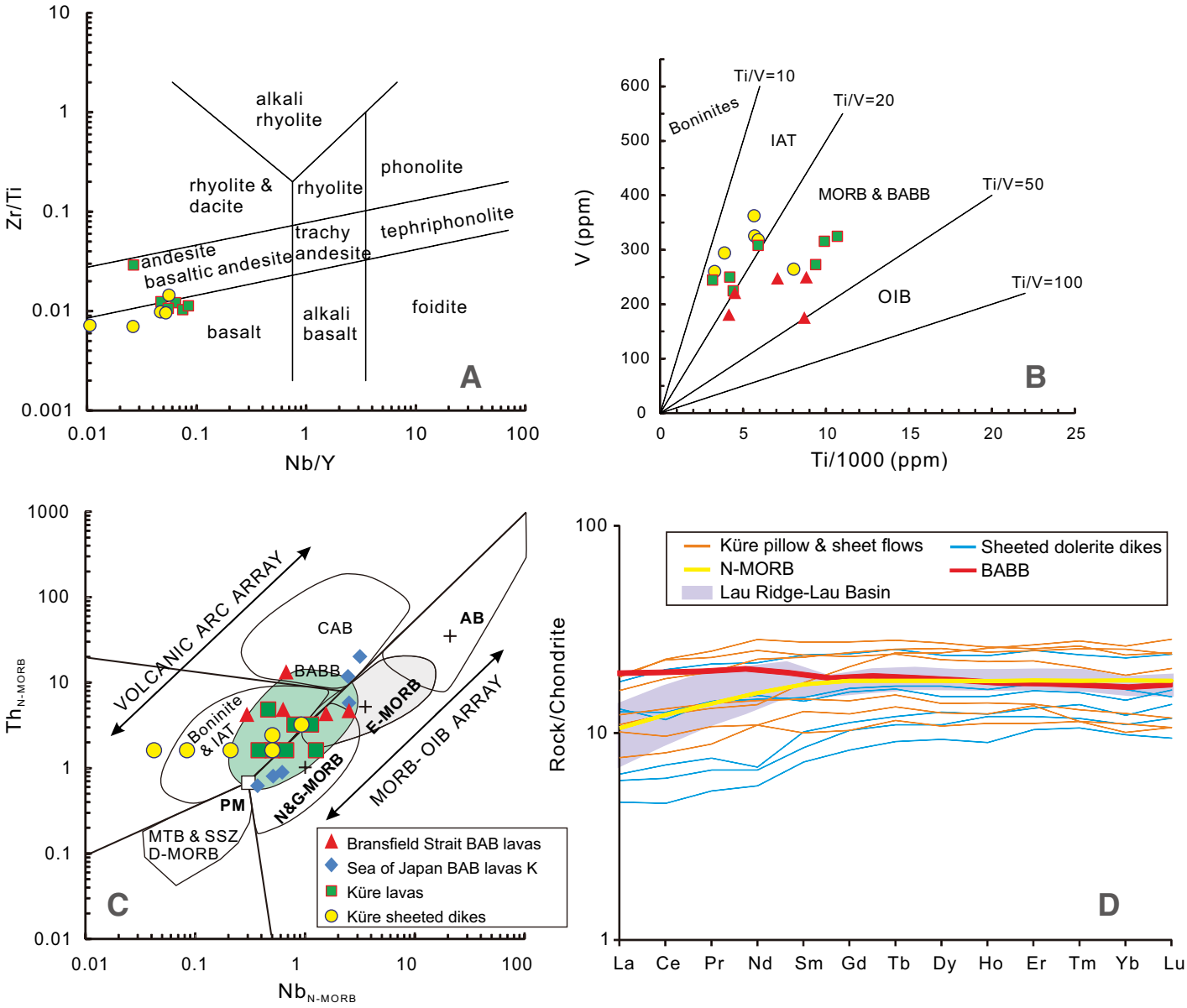

Figure 18. (A) Bivariate Nb/Y versus Zr/Ti discrimination diagram (Winchester and Floyd, 1977) for a representative suite of extrusive and sheeted dike rocks from the Küre ophiolite. (B) Ti versus V discrimination diagram (Shervais (1982) for a representative suite of extrusive and sheeted dike rocks from the Küre ophiolite in comparison to representative lava samples from the modern Bransfield Strait in northern Antarctica. Data for the Bransfield Strait lavas are from Keller et al. (2002). IAT—island arc tholeiite; BABB—backarc basin basalt; MORB—mid-oceanic ridge basalt; OIB—ocean island basalt. (C) Th_N-Nb_N discrimination diagram for a representative suite of extrusive and sheeted dike rocks from the Küre ophiolite in comparison to representative lava samples from the modern Sea of Japan (Yamato subbasin) and the Bransfield Strait (Antarctica). Diagram is from Saccani (2015). Data for the Bransfield Strait lavas are from Keller et al. (2002), and for the Sea of Japan (Yamato subbasin) lavas are from Hirahara et al. (2015). See text for discussion. MORB—N is normal; E is enriched; D is depleted; and G is garnet-influenced. CAB is calc-alkaline basalt; MTB is Medium-Ti basalt; SSS is suprasubduction zone. (D) Chondrite-normalized rare earth element concentration diagram for a representative suite of extrusive and sheeted dike rocks in the Küre ophiolite in comparison to the average N-MORB and BABB patterns, and to the Lau Ridge and Lau Basin lava field. Data for the Bransfield Strait lavas are from Keller et al. (2002), and for the Sea of Japan (Yamato subbasin) lavas are from Hirahara et al. (2015). Chondrite normalization values are from Sun and McDonough (1989). Average BABB pattern is from Gale et al. (2013). See text for discussion.

west-northwest–east-southeast–oriented (in present coordinates) seafloor spreading center in a continental backarc basin during the Middle Jurassic (168 Ma). The west-northwest–east-southeast and northeast-southwest orientation of the sheeted dike intrusions and low- to high-angle mineralized normal faults within the gabbros, sheeted dikes, and extrusive rock units strongly support the seafloor spreading origin of the Küre ophiolite. Fault-bound, wide alteration zones within the extrusive sequence are reminiscent of hydrothermal discharge zones along modern seafloor spreading centers (Fig. 7; Rona et al., 1993; Humphris et al., 1995; Thurnherr and Richards, 2001). The occurrence of the Küre volcanogenic massive sulfide deposit is analogous to Besshi-type massive sulfide deposits of modern and paleo–backarc basin examples (Slack, 1993) and to massive sulfide ore mineralization at sediment-buried mid-ocean ridges (Shanks and Thurston, 2012). The northwest-southeast– and northeast-southwest–oriented, oblique-slip fault systems documented in the sheeted dike complex and the extrusive sequence represent spreading-parallel and spreading-perpendicular strike-slip faults.

The uppermost part of the extrusive sequence is stratigraphically transitional into an argillite and then into sandstone-siltstone-shale turbiditic deposits without a tectonic discontinuity. These siliciclastic rocks are locally interleaved with pillow and massive lava flows and contain disseminated thin layers of massive sulfide mineralization zones. Blocks of pillow breccias and hyaloclastite rocks in the argillite and black shale (Fig. 9) indicate their origin as olistoliths from local igneous basement highs (i.e., fault-bound horsts of volcanic rocks). The upsection increase of clayey siltstone and mudstone rocks, which locally unconformably overlie the coarse-grained turbidites, suggests relatively low energy deposition in the basin, possibly at a post-spreading stage of the basin evolution. This stratigraphic sequence in the Küre sedimentary cover is similar to the depositional record of some of the modern marginal basins in the western Pacific region (Carey and Sigurdsson, 1984).

One of the best examples of continental backarc basins, as a modern analogue for the Küre basin, is the Sea of Japan in the northwest Pacific. The Sea of Japan started opening ca. 30 Ma as a result of the oblique subduction of the Pacific plate beneath the eastern Asian continental margin and the associated slab rollback (Tamaki, 1995). Drill cores obtained during Ocean Drilling Program Legs 127 and 128 in the Japan (Site 795) and Yamato subbasins (Sites 794 and 797) within the Sea of Japan have shown the occurrence of more than 900-m-thick (below the seafloor) basaltic lava flows, hyaloclastites, and brecciated basalts intercalated with and conformably overlain by laminated-bedded sandstone, siltstone, claystone, and black shale (Allan and Gorton, 1992; Hirahara et al., 2015). The clastic material in these sedimentary rocks appears to have been derived largely from the Asian continent during the rift-drift and seafloor spreading origin of the Sea of Japan (Marsaglia et al., 1995).

Sandstone layers in the sedimentary cover overlying the Küre ophiolite contain Paleoproterozoic and Archean detrital zircon grains derived from the East Europe continent, particularly from the Ukrainian shield. The occurrence of the Archean (3386 ± 124 Ma, 2715 ± 68 Ma, 2683 ± 98 Ma; Fig. 17C) detrital zircons indicates a close proximity of the Küre basin to an exposed Archean crystalline basement source area at the time of its seafloor spreading evolution.

Geodynamic Model

By the end of the Cimmeride orogeny, which resulted in the accretion of Permian–Triassic oceanic terranes to the southern margin of Eurasia in the Early Jurassic, a renewed subduction system dipping northward beneath the young Cimmeride orogenic belt was established and a new magmatic arc was developed along the southern margin of Eurasia (Fig. 19A; Okay and Nikishin, 2015). The positively buoyant continental upper plate and the old subducting oceanic plate with a high negative buoyancy led to rapid trench retreat and slab rollback (Holt et al., 2015). This geodynamic process resulted in the upper plate extension causing rifting and backarc basin opening and the migration of arc magmatism to the south (Fig. 19B). Within this north-facing subduction-accretion system, subduction-driven hydration and magmatism, asthenospheric upwelling, and decompression melting of the convecting mantle produced the forearc, arc, and backarc magmatism (respectively) with their characteristic geochemical fingerprints. A small continental sliver (Devrekani Massif) that separated from the Istanbul zone of Eurasia (Ustaömer and Robertson, 1994) during the initial stages of continental rifting was drifted away during the opening of the Küre backarc basin (Fig. 19B).

Relatively undeformed, uppermost Jurassic–Cretaceous shallow-marine carbonate rocks with a basal conglomerate unconformably overlie the Küre ophiolite and its sedimentary cover (Altun et al., 1990; Ustaömer and Robertson, 1994; this study). This observation suggests that the Küre basin was already into the advanced stages of its closure by the Early Cretaceous. Both north- and south-directed reverse and thrust faults and tight to isoclinal southward overturned folds in the turbiditic deposits were manifested during the north-south–directed contraction of the basin. The strongly developed south-vergent thrust-reverse fault kinematics recorded in the sedimentary cover rocks might have also developed, in part, during the collision of the Sakarya terrane with the Anatolide-Tauride Platform in the latest Cretaceous–early Cenozoic (Dilek and Sandvol, 2009; Okay, 2008).

CONCLUSIONS

The Küre ophiolite in the Sakarya terrane in northern Anatolia includes a complete ophiolite sequence (Penrose type) consisting of upper mantle peridotites, a transitional Moho layer, layered to isotropic gabbros, sheeted dikes, and an extrusive sequence. The total thickness of the crustal section of the ophiolite is ~5 km. Unlike in many other Tethyan ophiolites, which have pelagic depositional rocks (chert, radiolarite, chalk, and/or micritic limestone) as their in situ sedimentary cover, the Küre ophiolite is conformably overlain by turbiditic sandstone-siltstone-shale deposits, locally interleaved with pillow and massive lava flows and disseminated massive sulfide deposits. The thickness of this siliciclastic sedimentary cover sequence is ~3 km.

Dominantly west-northwest–east-southeast–oriented sheeted dikes and ductile to brittle extensional shear zones and normal faults within the lower crustal gabbroic rocks, the sheeted dike complex, and the extrusive sequence indicate a west-northwest–east-southeast–oriented (in present coordinates) paleo–seafloor spreading system along which the Küre oceanic crust was produced. The occurrence of volcanogenic massive sulfide deposits within the extrusive sequence and at the volcanic rock–sedimentary cover interface is analogous to hydrothermal discharge zones and the associated ore body deposits in modern backarc basins and sediment-buried mid-ocean ridge systems.

The U-Pb LA-ICP-MS zircon dating of an isotropic gabbro sample from the Küre ophiolite has revealed a concordant $^{206}Pb/^{238}U$ age of 168.8 ± 2.0 Ma; this new date constrains the timing of igneous construction of the ophiolite as the Middle Jurassic.

A careful evaluation of the regional geology, the internal structure, and the newly obtained isotopic age of the Küre ophiolite within the context of the tectonic architecture of the central Sakarya terrane points to its backarc basin origin above a north-dipping subduction zone. The geochemistry of the lava and dike rocks in the Küre ophiolite show MORB-like to IAT-like signatures with slight LREE enrichment patterns, typical of modern backarc basin lavas, and is consistent with a tectonically constrained backarc basin setting of the ophiolite formation.

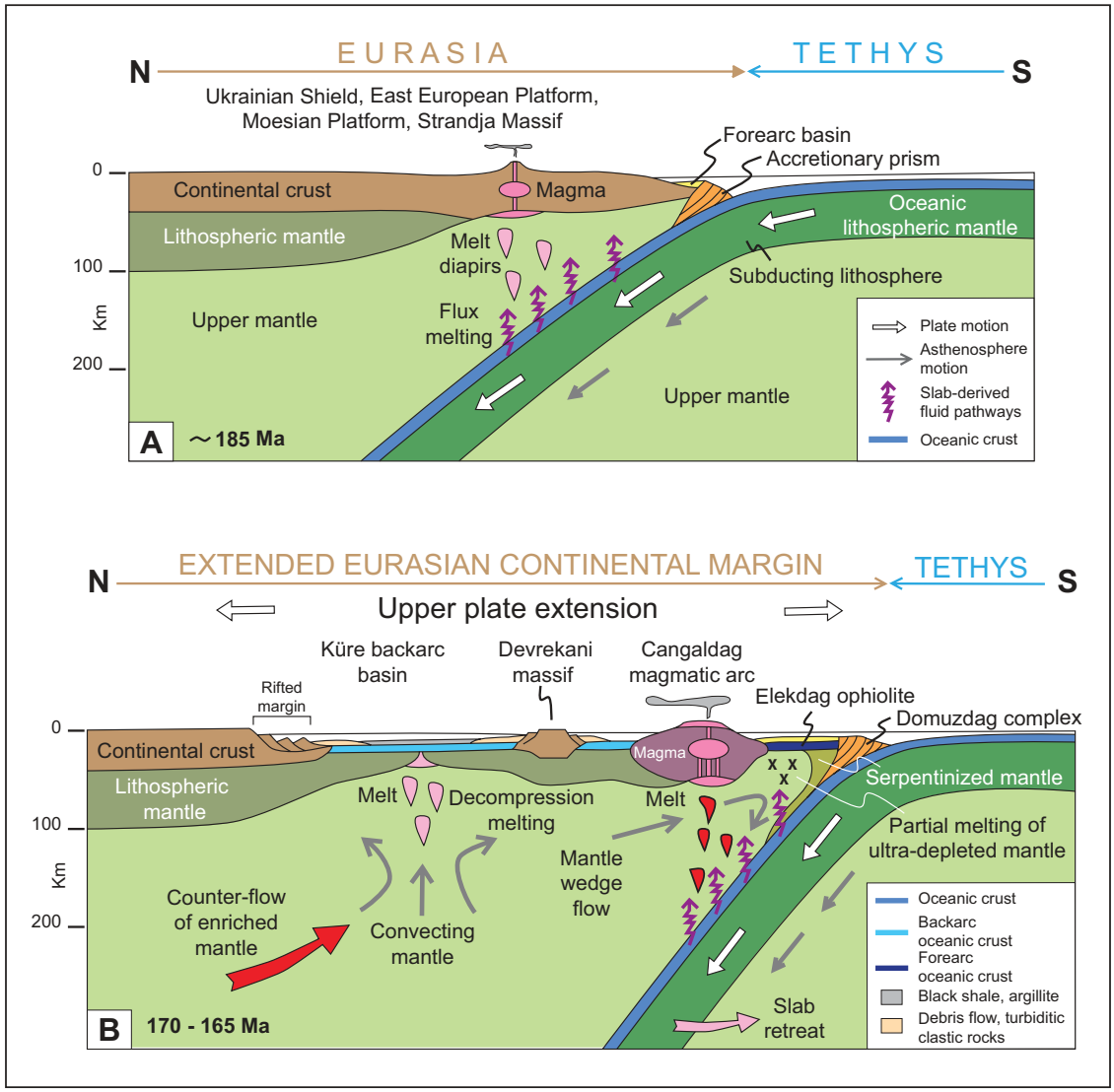

Figure 19. Tectonic model for the rift-drift and seafloor spreading evolution of the Küre continental backarc basin above a Tethyan subduction zone dipping northward beneath southern Eurasia. See text for discussion.

The U-Pb LA-ICP-MS dating of detrital zircons from a sandstone sample in the sedimentary cover of the Küre ophiolite has revealed the occurrence of Paleoarchean, Neoarchean, and Proterozoic zircons, as well as Paleozoic and early Mesozoic ones. These inherited Archean zircons were derived from the Eastern European Platform and/or the Ukrainian shield that are currently situated north and west of the modern Black Sea backarc basin. It is thus inferred that the Middle Jurassic Küre backarc basin developed proximal to the exposed Archean and Proterozoic terranes in the Eurasian continental realm. The Küre ophiolite represents a continental backarc basin oceanic lithosphere, reminiscent of the Cenozoic oceanic lithosphere in the modern Sea of Japan backarc basin.

ACKNOWLEDGMENTS

We thank Cüneyt Akal (Dokuz Eylül University, Izmir, Turkey) for giving us access to his zircon separation laboratory during the course of this study, and Ender Sarifakioglu (General Directorate of Mineral Exploration Institute, Ankara, Turkey) for her logistical help with our field work in Küre. The Turkish Petroleum Corporation provided financial support for the field work of Alparslan and Dilek in Turkey. This paper is part of the Alparslan's M.S. thesis (Miami University, Oxford, Ohio). We thank three anonymous referees for their insightful and constructive reviews of our manuscript for *Lithosphere*. We gratefully acknowledge the consideration and editorial handling of the Science Editor, Damian Nance.

REFERENCES CITED

Akbayram, K., Okay, A.I., and Satır, M., 2013, Early Cretaceous closure of the Intra Pontide Ocean in western Pontides (northwestern Turkey): Journal of Geodynamics, v. 65, p. 38–55, https://doi.org/10.1016/j.jog.2012.05.003.

Allan, J.F., and Gorton, M.P., 1992, Geochemistry of igneous rocks from Legs 127 and 128, Sea of Japan, *in* Tamaki, K., et al., eds., Proceedings of the Ocean Drilling Program, Scientific Results, Volume 127/128: College Station, Texas, Ocean Drilling Program, p. 905-929, https://doi.org/10.2973/odp.proc.sr.127128-2.208.1992.

Altherr, R., Topuz, G., Marschall, H., Zack, T., and Ludwig, T., 2004, Evolution of a tourmaline-bearing lawsonite eclogite from the Elekdağ area (Central Pontides, N Turkey): Evidence for infiltration of slab-derived B-rich fluids during exhumation: Contributions to Mineralogy and Petrology, v. 148, p. 409–425, https://doi.org/10.1007/s00410-004-0611-1.

Altun, I., Sengün, M., Keskin, H., Akçören, F., Sevin, M., Deveciler, E., and Akat, M.U., 1990, Kastamonu–B17 Quadrangle Geological Map: Ankara, Mineral Research and Exploration Directorate of Turkey, scale 1:100,000, 18 p.

Andersen, T., 2002, Correction of common lead in U-Pb analyses that do not report ^{204}Pb: Chemical Geology, v. 192, p. 59–79.

Anonymous, 1972, Penrose Field Conference on ophiolites: Geotimes, v. 17, p. 24–25.

Boztug, D., Debon, F., Le Fort, P., and Yilmaz, O., 1984, Geochemical characteristics of some plutons from the Kastamonu granitoid belt (northern Anatolia, Turkey): Schweizerische Mineralogische und Petrographische Mitteilungen, v. 64, p. 389–403.

Çakir, U., Genç, Y., and Paktunç, D., 2006, Intrusive lherzolites within the basalts of Küre ophiolite (Turkey): An occurrence in the Tethyan suprasubduction marginal basin: Geological Journal, v. 41, p. 123–143, https://doi.org/10.1002/gj.1037.

Carey, S., and Sigurdsson, H., 1984, A model of volcanogenic sedimentation in marginal basins, *in* Kokelaar, B.P., and Howells, M.F., eds., Marginal Basin Geology: Volcanic and Associated Sedimentary and Tectonic Processes in Modern and Ancient Marginal Basins: Geological Society of London Special Publication 16, p. 37–58, https://doi.org/10.1144/GSL.SP.1984.016.01.04.

Çelik, O.F., and Delaloye, M., 2003, Origin of metamorphic soles and their post-kinematic mafic dyke swarms in the Antalya and Lycian ophiolites, SW Turkey: Geological Journal, v. 38, p. 235–256, https://doi.org/10.1002/gj.954.

Çimen, O., 2016, Petrology and geochronology of the igneous rocks from the Çangaldag metamorphic complex and the Çangaldag Pluton (Central Pontides, Turkey) [Ph.D. thesis]: Ankara, Turkey, Middle East Technical University, 282 p., http://etd.lib.metu.edu.tr/upload/12620274/index.pdf.

Claesson, S., Bibikova, E., Bogdanova, S., and Skobelev, V., 2006, Archaean terranes, Paleoproterozoic reworking and accretion in the Ukrainian shield, East European Craton, *in* Gee, D.G., and Stephenson, R.A., eds., European Lithosphere Dynamics: Geological Society of London Memoir 32, p. 645–654, https://doi.org/10.1144/GSL.MEM.2006.32.01.38.

Coogan, L.A., Howard, K.A., Gillis, K.M., Bickle, M.J., Chapman, H.J., Boyce, A.J., Jenkin, G.R.T., and Wilson, R.N., 2006, Chemical and thermal constraints on focussed fluid flow in the lower oceanic crust: American Journal of Science, v. 306, p. 389–427, https://doi.org/10.2475/06.2006.01.

Cowan, D.S., 1985, Structural styles in Mesozoic and Cenozoic melanges in the Western Cordillera of North America: Geological Society of America Bulletin, v. 96, p. 451–462, https://doi.org/10.1130/0016-7606(1985)96<451:SSIMAC>2.0.CO;2.

Dean, W.T., Monod, O., Rickards, R.B., Demir, O., and Bultynck, P., 2000, Lower Paleozoic stratigraphy and paleontology, Karadere-Zirze area, Pontus Mountains, northern Turkey: Geological Magazine, v. 137, p. 555–582, https://doi.org/10.1017/S0016756800004635.

Dilek, Y., 2003a, Ophiolites, mantle plumes and orogeny, *in* Dilek, Y., and Robinson, P.T., eds., Ophiolites in Earth History: Geological Society of London Special Publication 218, p. 9–19, https://doi.org/10.1144/GSL.SP.2003.218.01.02.

Dilek, Y., 2003b, Ophiolite concept and its evolution, *in* Dilek, Y., and Newcomb, S., eds., Ophiolite Concept and the Evolution of Geological Thought: Geological Society of America Special Paper 373, p. 1–16, https://doi.org/10.1130/0-8137-2373-6.1.

Dilek, Y., 2006, Collision tectonics of the Eastern Mediterranean region: Causes and consequences, *in* Dilek, Y., and Pavlides, S., eds., Postcollisional Tectonics and Magmatism in the Mediterranean Region and Asia: Geological Society of America Special Paper 409, p. 1–13, https://doi.org/10.1130/2006.2409(01).

Dilek, Y., and Delaloye, M., 1992, Structure of the Kizildag ophiolite, a slow-spread Cretaceous ridge segment north of the Arabian promontory: Geology, v. 20, p. 19–22. https://doi.org/10.1130/0091-7613(1992)020<0019:SOTKOA>2.3.CO;2.

Dilek, Y., and Eddy, C.A., 1992, The Troodos (Cyprus) and Kizildag (S. Turkey) ophiolites as structural models for slow-spreading ridge segments: Journal of Geology, v. 100, p. 305–322, https://doi.org/10.1086/629634.

Dilek, Y., and Furnes, H., 2011, Ophiolite genesis and global tectonics: Geochemical and tectonic fingerprinting of ancient oceanic lithosphere: Geological Society of America Bulletin, v. 123, p. 387–411, https://doi.org/10.1130/B30446.1.

Dilek, Y., and Furnes, H., 2014, Ophiolites and their origins: Elements, v. 10, p. 93–100, https://doi.org/10.2113/gselements.10.2.93.

Dilek, Y., and Moores, E.M., 1990. Regional tectonics of the Eastern Mediterranean ophiolites, *in* Malpas, J., et al., eds., Ophiolites, Oceanic Crustal Analogues: Proceedings of the Symposium Troodos 1987: Nicosia, Cyprus, Geological Survey Department, p. 295–309.

Dilek, Y., and Sandvol, E., 2009, Seismic structure, crustal architecture and tectonic evolution Anatolian-African plate boundary and the Cenozoic orogenic belts in the eastern Mediterranean region, *in* Murphy, J.B., et al., eds., Ancient Orogens and Modern Analogues: Geological Society of London Special Publications, v. 327, p. 127–160, https://doi.org/10.1144/SP327.8.

Dilek, Y., and Thy, P., 1998, Structure, petrology, and seafloor spreading tectonics of the Kizildag ophiolite (Turkey), *in* Mills, R., and Harrison, K., eds., Modern Ocean Floor Processes and the Geological Record: Geological Society of London Special Publication 148, p. 43–69, https://doi.org/10.1144/GSL.SP.1998.148.01.04.

Dilek, Y., and Whitney, D.L., 2000, Cenozoic crustal evolution in central Anatolia: Extension, magmatism and landscape development: Proceedings of the Third International Conference on the Geology of the Eastern Mediterranean: Nicosia, Cyprus, Geological Survey Department, p. 183–192.

Dilek, Y., Thy, P., Hacker, B., and Grundvig, S., 1999, Structure and petrology of Tauride ophiolites and mafic dike intrusions (Turkey): Implications for the Neo-Tethyan ocean: Geological Society of America Bulletin, v. 111, p. 1192–1216, https://doi.org/10.1130/0016-7606(1999)111<1192:SAPOTO>2.3.CO;2.

Dilek, Y., Furnes, H., and Shallo, M., 2008, Geochemistry of the Jurassic Mirdita Ophiolite (Albania) and the MORB to SSZ evolution of a marginal basin oceanic crust: Lithos, v. 100, p. 174–209, https://doi.org/10.1016/j.lithos.2007.06.026.

Dilek, Y., Imamverdiyev, N., and Altunkaynak, S., 2010, Geochemistry and tectonics of Cenozoic volcanism in the Lesser Caucasus (Azerbaijan) and the peri-Arabian region: Collision-induced mantle dynamics and its magmatic fingerprint: International Geology Review, v. 52, p. 536–578, https://doi.org/10.1080/00206810903360422.

Dönmez, C., Keskin, S., Günay, K., Çolakoglu, A.O., Çiftçi, Y., Uysal, I., Türkel, A., and Yildirim, N., 2014, Chromite and PGE geochemistry of the Elekdag ophiolite (Kastamonu, northern Turkey): Implications for deep magmatic processes in a supra-subduction zone setting: Ore Geology Reviews, v. 57, p. 216–228, https://doi.org/10.1016/j.oregeorev.2013.09.019.

Elmas, A., and Yiğitbaş, E., 2001, Ophiolite emplacement by strike-slip tectonics between the Pontide Zone and the Sakarya Zone in northwestern Anatolia, Turkey: International Journal of Earth Sciences, v. 90, p. 257–269, https://doi.org/10.1007/s005310000129.

Ewart, A., Collerson, K.D., Regelous, M., Wendt, J.I., and Niu, Y., 1998, Geochemical evolution within the Tonga–Kermadec–Lau Arc back-arc systems: The role of varying mantle wedge composition in space and time: Journal of Petrology, v. 39, p. 331–368, https://doi.org/10.1093/petroj/39.3.331.

Festa, A., Pini, G.A., Dilek, Y., and Codegone, G., 2010, Mélanges and mélange-forming processes: A historical overview and new concepts: International Geology Review, v. 52, p. 1040–1105, https://doi.org/10.1080/00206810903557704.

Festa, A., Ogata, K., Pini, G.A., Dilek, Y., and Alonso, J.L., 2016, Origin and significance of olistostromes in the evolution of orogenic belts: A global synthesis: Gondwana Research, v. 39, p. 180–203, https://doi.org/10.1016/j.gr.2016.08.002.

Flower, M.F.J., 2003, Ophiolites, historical contingency, and the Wilson cycle, *in* Dilek, Y., and Newcomb, S., eds., Ophiolite Concept and the Evolution of Geological Thought: Geological Society of America Special Paper 373, p. 111–135, https://doi.org/10.1130/0-8137-2373-6.111.

Furnes, H., de Wit, M., and Dilek, Y., 2014, Four billion years of ophiolites reveal secular trends in oceanic crust formation: Geoscience Frontiers, v. 5, p. 571–603, https://doi.org/10.1016/j.gsf.2014.02.002.

Gale, A., Dalton, C.A., Langmuir, C.H., Su, Y., and Schilling, J.G., 2013, The mean composition of ocean ridge basalts: Geochemistry, Geophysics, Geosystems, v. 14, p. 489–518, https://doi.org/10.1029/2012GC004334.

Göncüoglu, M.C., Marroni, M., Sayit, K., Tekin, U.K., Ottri, A., Pandolfi, L., and Ellero, A., 2012, The Ayli Dag ophiolite sequence (central-northern Turkey): A fragment of middle Jurassic oceanic lithosphere within the Intra-Pontide suture zone: Ofioliti, v. 37, p. 77–91, https://doi.org/10.4454/ofioliti.v37i2.407.

Görür, N., Monod, O., Okay, A.I., Sengör, A.M.C., Tüysüz, O., Yigitbas, E., Sakinç, M., and Akkok, R., 1997, Paleogeographic and tectonic position of the Carboniferous rocks of the western Pontides (Turkey) in the frame of the Variscan belt: Bulletin de la Société Géologique de France, v. 168, p. 197–205.

Güner, M., 1980, Massive sulphide ores and geology of the Küre area, Pontides (N. Turkey): Maden Tetkik ve Arama Enstitüsü Bülteni, v. 93/94, p. 65–109.

Harper, G.D., Saleeby, J.B., and Heizler, M., 1994, Formation and emplacement of the Josephine ophiolite and the Nevadan orogeny in the Klamath Mountains, California-Oregon: U-Pb zircon and $^{40}Ar/^{39}Ar$ geochronology: Journal of Geophysical Research, v. 99, p. 4293–4321, https://doi.org/10.1029/93JB02061.

Hawkins, J.W., 1977, Petrologic and geochemical characteristics of marginal basin basalts, *in* Talwani, M., and Pitman, W.C., III, eds., Island Arcs, Deep Sea Trenches and Back Arc Basins: Maurice Ewing Series Volume 1: Washington, D.C., American Geophysical Union, p. 355–365, https://doi.org/10.1029/ME001p0355.

Hawkins, J.W., 2003, Geology of supra-subduction zones—Implications for the origin of ophiolites, *in* Dilek, Y., and Newcomb, S., eds., Ophiolite Concept and the Evolution of Geological Thought: Geological Society of America Special Paper 373, p. 227–268, https://doi.org/10.1130/0-8137-2373-6.227.

Hirahara, Y., Kimura, J., Senda, R., Miyazaki, T., Kawabata, H., Takahashi, T., Chang, Q., Vaglarov, B.S., Sato, T., and Kodaira, S., 2015, Geochemical variation in Japan Sea backarc basin basalts formed by high-temperature adiabatic melting of mantle metasomatized by sediment subduction components: Geochemistry, Geophysics, Geosystems, v. 16, p. 1324–1347, https://doi.org/10.1002/2015GC005720.

Hofmann, A., and Wilson, A.H., 2007, Silicified basalts, bedded cherts and other sea floor alteration phenomena of the 3.4 Ga Nondweni Greenstone Belt, South Africa, *in* Van Kranendonk, M., et al., eds., Developments in Precambrian Geology: Amsterdam, Elsevier, p. 571–605, https://doi.org/10.1016/S0166-2635(07)15055-6.

Holt, A.F., Becker, T.W., and Buffett, B.A., 2015, Trench migration and overriding plate stress in dynamic subduction models: Geophysical Journal International, v. 201, p. 172–192, https://doi.org/10.1093/gji/ggv011.

Humphris, S.E., et al., 1995, The internal structure of an active seafloor massive sulphide deposit: Nature, v. 377, p. 713–716, https://doi.org/10.1038/377713a0.

Jolivet, L., Tamaki, K., and Fournier, M., 1994, Japan Sea, opening history and mechanism: A synthesis: Journal of Geophysical Research, v. 99, p. 22,237–22,259, https://doi.org/10.1029/93JB03463.

Keller, R.A., Fisk, M.R., Smellie, J.L., Strelin, J.A., Lawve, L.A., and White, W.M., 2002, Geochemistry of back arc basin volcanism in Bransfield Strait, Antarctica: Subducted contributions and along-axis variations: Journal of Geophysical Research, v. 107, p. ECV 4-1–ECV 4-17, https://doi.org/10.1029/2001JB000444.

Kovenko, V., 1944, Metallogeny of the old copper body in Küre and recently discovered Asiköy body in the central and eastern coastal parts of the Black Sea region: Maden Tetkik ve Arama Enstitüsü Bülteni, v. 2/32, p. 180–212.

Kozur, H., Aydin, M., Demir, O., Yakar, H., Goncuoglu, M.C., and Kuru, F., 2000, New stratigraphic and paleogeographic results from the Paleozoic and early Mesozoic of the Middle Pontide (northern Turkey) in the Azdavay, Devrekani, Küre and Inebolu areas: Implications for the Carboniferous–Early Cretaceous geodynamic evolution and some related remarks to the Karakaya oceanic rift basin: Geologia Croatica, v. 53, p. 209–268.

Kusçu, I., and Erler, A., 2002, Pyrite deformation textures in the deposits of the Küre mining district (Kastamonu–Turkey): Turkish Journal of Earth Sciences, v. 11, p. 205–215.

Lanson, B., Sakharov, B.A., Claret, F., and Drits, V.A., 2009, Diagenetic smectite-to-illite transition in clay-rich sediments: A reappraisal of X-ray diffraction results using the multi-specimen method: American Journal of Science, v. 309, p. 476–516, https://doi.org/10.2475/06.2009.03.

Marroni, M., Frassi, C., Goncuoglu, M.C., Di Vincenzo, G., Pandolfi, L., Rebay, G., Ellero, A., and Ottria, G., 2014, Late Jurassic amphibolite-facies metamorphism in the Intra-Pontide

Suture Zone (Turkey): An eastward extension of the Vardar Ocean from the Balkans into Anatolia?: Journal of the Geological Society [London], v. 171, p. 605–608, https://doi.org/10.1144/jgs2013-104.

Marsaglia, K.M., Boggs, S., Clift, P.D., Seyeolali, A., and Smith, R., 1995, Sedimentation in Western Pacific Basins: New insights from recent ODP drilling, *in* Taylor, B., and Natland, J., eds., Active Margins and Marginal Basins of the Western Pacific: American Geophysical Union Geophysical Monograph 88, p. 291–314, https://doi.org/10.1029/GM088p0291.

McCollom, T.M., and Shock, E.L., 1998, Fluid-rock interactions in the lower oceanic crust: Thermodynamic models of hydrothermal alteration: Journal of Geophysical Research, v. 103, p. 547–575, https://doi.org/10.1029/97JB02603.

Mints, M.V., 2015, Northeastern part of the Archean Sarmatia continent, *in* Mints, M.V., et al., eds., East European Craton: Early Precambrian History and 3D Models of Deep Crustal Structure: Geological Society of America Special Paper 510, p. 125–129, https://doi.org/10.1130/2015.2510(04).

Mints, M.V., Philippova, I.B., Babayants, P.S., Blokh, Y.I., and Trusov, A.A., 2015. Middle Paleoproterozoic Bryansk-Kursk-Voronezh intracontinental collisional orogen, *in* Mints, M.V., et al., eds., East European Craton: Early Precambrian History and 3D Models of Deep Crustal Structure: Geological Society of America Special Paper 510, p. 155–169, https://doi.org/10.1130/2015.2510(06).

Moix, P., Beccaletto, L., Kozur, H.W., Hochard, C., Rosselet, F., and Stampfli, G.M., 2008, A new classification of the Turkish terranes and sutures and its implication for the paleotectonic history of the region: Tectonophysics, v. 451, p. 7–39, https://doi.org/10.1016/j.tecto.2007.11.044.

Moores, E.M., 1982, Origin and emplacement of ophiolites: Reviews of Geophysics and Space Physics, v. 20, p. 735–760, https://doi.org/10.1029/RG020i004p00735.

Nakayama, K., and Kaya, N., 1999, The Küre VMS (volcanogenic massive sulfide) deposit associated with the paleo-Tethys ophiolite, Turkey: Allochthonous sulfide ore blocks in terrigenous sedimentary rocks: Chishitsugaku Zasshi, v. 105, no. 5, p. IX–X.

Nikishin, A.M., Okay, A.I., Tuysuz, O., Demirer, A., Wannier, M., Amelin, N., and Petrov, E., 2015, The Black Sea basins structure and history: New model based on new deep generation regional seismic data. Part 1: Basins structure and fill: Marine and Petroleum Geology, v. 59, p. 638–655, https://doi.org/10.1016/j.marpetgeo.2014.08.017.

Nzegge, O.M., 2008, Petrogenesis and geochronology of the Deliktas, Sivrikaya and Devrekani granitoids and basement, Kastamonu belt, Central Pontides (NW Turkey): Evidence for late Paleozoic–Mesozoic plutonism and geodynamic interpretation [Ph.D. thesis]: Tübingen, Germany, Institut für Geowissenschaften Universität Tübingen, 177 p.

Okay, A.I., 2008, Geology of Turkey: A Synopsis: Anschnitt, v. 21, p. 19–42.

Okay, A.I., and Nikishin, A.M., 2015, Tectonic evolution of the southern margin of Laurasia in the Black Sea region: International Geology Review, v. 57, p. 1051-1076, https://doi.org/10.1080/00206814.2015.1010609.

Okay, A.I., and Şahintürk, Ö., 1997, Geology of the Eastern Pontides, *in* Robinson, A.G., ed., Regional and Petroleum Geology of the Black Sea and Surrounding Region: American Association of Petroleum Geologists Memoir 68, p. 291–311,.

Okay, A.I., and Tüysüz, O., 1999, Tethyan sutures of northern Turkey, *in* Durand, B., et al., eds., The Mediterranean Basins: Tertiary Extension within the Alpine Orogen: Geological Society of London Special Publication 156, p. 475–515, https://doi.org/10.1144/GSL.SP.1999.156.01.22.

Okay, A.I.O., Monod, O., and Monié, P., 2002, Triassic blueschists and eclogites from northwest Turkey: Vestiges of the Paleo-Tethyan subduction: Lithos, v. 64, p. 155–178, https://doi.org/10.1016/S0024-4937(02)00200-1.

Okay, A.I., Tüysüz, O., Satir, M., Özkan-Altiner, S., Altinner, D., Sherlock, S., and Eren, R.H., 2006, Cretaceous and Triassic subduction-accretion, HP/LT metamorphism and continental growth in the Central Pontides, Turkey: Geological Society of America Bulletin, v. 118, p. 1247–1269, https://doi.org/10.1130/B25938.1.

Okay, A.I., Sunal, G., Tüysüz, O., Keskin, M., and Kylander-Clark, A.R.C., 2014, Low-pressure–high-temperature metamorphism during extension in a Jurassic magmatic arc, Central Pontides, Turkey: Journal of Metamorphic Geology, v. 32, p. 49–69, https://doi.org/10.1111/jmg.12058.

Okay, A.I., Altiner, D., and Kilic, A.M., 2015, Triassic limestone, turbidities, and serpentinite—The Cimmeride orogeny in the Central Pontides: Geological Magazine, v. 152, p. 460–479, https://doi.org/10.1017/S0016756814000429.

Rassios, A.E., and Dilek, Y., 2008, Rotational deformation in the Jurassic Mesohellenic ophiolites, Greece, and its tectonic significance: Lithos, v. 108, p. 207–223, https://doi.org/10.1016/j.lithos.2008.09.005.

Robertson, A.H.F., 2002, Overview of the genesis and emplacement of Mesozoic ophiolites in the Eastern Mediterranean Tethyan region: Lithos, v. 65, p. 1–67, https://doi.org/10.1016/S0024-4937(02)00160-3.

Robinson, A.G., Banks, C.J., Rutherford, M.M., and Hirst, J.P.P., 1995, Stratigraphic and structural development of the Eastern Pontides, Turkey: Journal of the Geological Society [London], v. 152, p. 861–872, https://doi.org/10.1144/gsjgs.152.5.0861.

Rona, P.A., Hannington, M.D., Raman, C.V., Thompson, G., Tivey, M.K., Humphris, S.E., Lalou, C., and Petersen, S., 1993, Active and relic sea-floor hydrothermal mineralization at the TAG hydrothermal field, Mid-Atlantic Ridge: Economic Geology and the Bulletin of the Society of Economic Geologists, v. 88, p. 1989–2017, https://doi.org/10.2113/gsecongeo.88.8.1989.

Saccani, E., 2015, A new method of discriminating different types of post-Archean ophiolitic basalts and their tectonic significance using Th-Nb and Ce-Dy-Yb systematics: Geoscience Frontiers, v. 6, p. 481–501, https://doi.org/10.1016/j.gsf.2014.03.006.

Sarıfakıoğlu, E., Dilek, Y., and Sevin, M., 2017, New synthesis of the Izmir-Ankara-Erzincan suture zone and the Ankara mélange in northern Anatolia based on new geochemical and geochronological constraints, *in* Sorkhabi, R., ed., Tectonic Evolution, Collision, and Seismicity of Southwest Asia: In Honor of Manuel Berberian's Forty-Five Years of Research Contributions: Geological Society of America Special Paper 525, https://doi.org/10.1130/2017.2525(19).

Schellart, W.P.S., and Lister, G.S., 2005, The role of the East Asian active margin in widespread extensional and strike-slip deformation in East Asia: Journal of the Geological Society [London], v. 162, p. 959–972, https://doi.org/10.1144/0016-764904-112.

Sdrolias, M., and Müller, R.D., 2006, Controls on back-arc basin formation: Geochemistry, Geophysics, Geosystems, v. 7, Q04016, doi:10.1029/2005GC001090.

Seyfried, W.E., Berndt, M.E., and Seewald, J.S., 1988, Hydrothermal alteration processes at mid-ocean ridges: Constraints from diabase alteration experiments, hot-spring fluids and composition of the oceanic crust: Canadian Mineralogist, v. 26, p. 787–804.

Shallo, M., and Dilek, Y., 2003, Development of the ideas on the origin of Albanian ophiolites, *in* Dilek, Y., and Newcomb, S., eds., Ophiolite Concept and the Evolution of Geological Thought: Boulder, Colorado, Geological Society of America Special Paper 373, p. 351–363, https://doi.org/10.1130/0-8137-2373-6.351.

Shanks, W.C.P., III, and Thurston, R., 2012, Volcanogenic massive sulfide occurrence: U.S. Geological Survey Scientific Investigations Report 2010-5070-C, 345 p.

Shervais, J.W., 1982, Ti-V plots and the petrogenesis of modern and ophiolitic lavas: Earth and Planetary Science Letters, v. 59, p. 101–118, https://doi.org/10.1016/0012-821X(82)90120-0.

Slack, J.F., 1993, Descriptive and grade-tonnage models for Besshi-type massive sulfide deposit, *in* Kirkham, R.V., et al., eds., Mineral Deposit Modeling: Geological Association of Canada Special Paper 40, p. 343–371.

Staudigel, H., and Hart, R., 1983, Alteration of basaltic glass: Mechanism and significance for the oceanic crust-seawater budget: Geochimica et Cosmochimica Acta, v. 47, p. 337–350, https://doi.org/10.1016/0016-7037(83)90257-0.

Stern, C., and de Wit, M.J., 2003, Rocas Verdes ophiolites, southernmost South America: Remnants of progressive stages of development of oceanic-type crust in a continental margin back-arc basin, *in* Dilek, Y., and Robinson, P.T., eds., Ophiolites in Earth History. Geological Society of London Special Publication 218, p. 665–683, https://doi.org/10.1144/GSL.SP.2003.218.01.32.

Sun, S., and McDonough, W., 1989, Chemical and isotopic systematics of oceanic basalts: Implications for mantle composition and processes, *in* Saunders, A.D., and Norry, M.J., eds., Magmatism in the Ocean Basins: Geological Society of London Special Publication 42, p. 313–345, https://doi.org/10.1144/GSL.SP.1989.042.01.19.

Sunal, G., Natal'in, B., Satir, M., and Toraman, E., 2006, Paleozoic magmatic events in the Strandja Massif, NW Turkey: Geodinamica Acta, v. 19, p. 283–300, https://doi.org/10.3166/ga.19.283-300.

Tamaki, K., 1995, Opening tectonics of the Japan Sea, *in* Taylor, B., ed., Backarc Basins. Tectonics and Magmatism: New York, Plenum Press, p. 407–420, https://doi.org/10.1007/978-1-4615-1843-3_11.

Tankut, A., Dilek, Y., and Önen, P., 1998, Petrology and geochemistry of the Neo-Tethyan volcanism as revealed in the Ankara Mélange, Turkey: Journal of Volcanology and Geothermal Research, v. 85, p. 265–284, https://doi.org/10.1016/S0377-0273(98)00059-6.

Thomas, W.A., 2011, Detrital-zircon geochronology and sedimentary provenance: Lithosphere, v. 3, p. 304–308, https://doi.org/10.1130/RF.L001.1.

Thurnherr, A.M., and Richards, K.J., 2001, Hydrography and high-temperature heat flux of the Rainbow hydrothermal site (36°14′N, Mid-Atlantic Ridge): Journal of Geophysical Research, v. 106, p. 9411–9426, https://doi.org/10.1029/2000JC900164.

Ustaömer, T., and Robertson, A.H.F., 1994, Late Paleozoic marginal basin and subduction-accretion: The Paleotethyan Kure Complex, Central Pontides, northern Turkey: Journal of the Geological Society [London], v. 151, p. 291–305, https://doi.org/10.1144/gsjgs.151.2.0291.

Winchester, J.A., and Floyd, P.A., 1977, Geochemical discrimination of different magma series and their differentiation products using immobile elements: Chemical Geology, v. 20, p. 325–343, https://doi.org/10.1016/0009-2541(77)90057-2.

Yamamato, Y., Tonogai, K., and Anma, R., 2011, Fabric-based criteria to distinguish tectonic from sedimentary mélanges in the Shimanto accretionary complex, Yakushima Island, SW Japan: Tectonophysics, v. 568, p. 65–73, 10.1016/j.tecto.2011.10.018.

Zagorchev, I., 2008, Amphibolite-facies metamorphic complexes in Bulgaria and Precambrian geodynamics: Controversies and "state of the art": Geologica Balcanica, v. 37, p. 33–46.

MANUSCRIPT RECEIVED 22 DECEMBER 2016
REVISED MANUSCRIPT RECEIVED 2 DECEMBER 2017
MANUSCRIPT ACCEPTED 15 DECEMBER 2017